REFLECT DELIVERABLE D2.6

ROLE OF MICROORGANISMS AND ORGANIC COMPOUNDS

Evaluating the effect of Organic Compounds and Microorganisms in formation and precipitation of Colloids using artificial brines

Summary:

The evaluation of the effect of organic compounds and microorganisms in formation and precipitation of colloids using artificial brines was performed by TNO using selected organic compounds based on the analysis of sampled fluids corresponding to the information gathered on the sites by GFZ. The same was done with biofilms prepared with microorganisms (*Thermaerobacter* sp., *Penicilium citrinum*) isolated from geothermal stations by UNINE. All carboxylic acids tested had an inhibiting effect on the precipitation of calcium carbonate. The biofilm components seem to develop intense interaction with the ions, nuclei and/or crystals formed during the executed experiments. In the presence of biofilms, the transformation of the intrinsically formed vaterite morphology to equilibrium calcite morphologies is delayed or hindered and scaling was inhibited.

Authors:

Hartmut Fischer, TNO, Senior Scientist; Andrea Vieth-Hillebrand, GFZ, Senior Scientist; Simona Regenspurg, GFZ, Senior Scientist; Alessio Leins, GFZ, PhD student; Pilar Junier, UNINE, Professor; Danae Bregnard, UNINE, PhD student

This project has received funding from the European Union's Horizon 2020 research and innovation programme under grant agreement nº 850626.

Title:	ROLE OF MICROORGANISMS AND ORGANIC COMPOUNDS
Lead beneficiary:	TNO
Other beneficiaries:	UNINE, GFZ
Due date:	30. 11. 2022
Nature:	Public
Diffusion:	all Partners
Status:	Final
Document code:	Reflect_D2.6
DOI:	10.48440/gfz.4.8.2022.004
License information:	CC-BY-4.0
Recommended citation:	H. Fischer, Bregnard, D., Leins, A., Vieth-Hillebrand, A., Regenspurg, S., Junier, P. The H2020 REFLECT project: *Deliverable_2.6- Role of microorganism and organic compounds, GFZ German Research Centre for Geosciences.* 2022 DOI: 10.48440/gfz.4.8.2022.004

Revision history	Author	Delivery date	Summary of changes and comments
Version 01	H. Fischer	17.06.2022	Summary experiments performed by TNO
Version 02	P. Junier	13.07.2022	Summary experiments performed by UNINE and comments in the previous version
Version 02	A. Vieth-Hillebrand	26.08.2022	Summary experiments performed by GFZ and comments in the previous version
Final version	All co-authors	23.09.2022	Final editing and proof-reading

Approval status				
	Name	Function	Date	Signature
Deliverable responsible	H. Fischer	Task member WP 2.5		
Deliverable responsible	A. Vieth-Hillebrand	Task member WP 2.5		
Task leader	P. Junier	Leader Task 2.5		
WP leader	C. Boeije	Leader WP2	28.10.2022	
Reviewer	Joseph Trimboli	Senior scientist TNO		
Reviewer	S. Regenspurg			
Project Coordinator	K. Kieling	Project manager	26.10.2022	

Table of contents

FIGURES

TABLES

1 EXECUTIVE SUMMARY

Bacterial growth has been observed at many heat-providing geothermal sites, but bacterial spores have been identified and revived even from sites with temperatures of up to 150 °C. Upon cooling of the brine, spores can reactivate and contribute to the formation of biofilms or provoke mineral precipitation. These two phenomena have the potential to impact fluid reinjection. Bacterial growth can be stimulated further by the presence of organic compounds. Sedimentary basin fluids frequently contain organic components, which explains why injectivity problems have been correlated with biofilms and very high dissolved concentrations of organic carbon (above 1000 mg/L). Consequently, a mitigation of microbial activity and prevention of the formation of organic scales requires knowledge about the roles that microorganisms and organic compounds play in geothermal brines.

The aim of the WP 2.5.2 was the evaluation of the effect of organic compounds and microorganisms in formation and precipitation of colloids using artificial brines. UNINE provided the biological material (active and inactive bacteria/fungi) from its culture collection (including strains isolated from geothermal brines), and a selection of organic compounds was made based on the analysis of the dissolved organic compounds from sampled fluids performed by GFZ. A method developed by TNO using dynamic light scattering (DLS) was used for the experiments. This approach has proven to be a new way to study important aspects of homogeneous nucleation like induction time and relative amounts of precipitate formed.

First, an investigation of the effect of several common carboxylic acids on the formation of homogeneous calcium carbonate scale was conducted. All carboxylic acids tested had an inhibitory effect on the precipitation of calcium carbonate. Both the induction time and amount of precipitation was influenced by the carboxylic acids tested. DLS results showed that an increase in acid concentration results in increased induction time and reduced total precipitation. Also, as the number of carboxylic groups in the acid molecule increases, less acid concentration is needed to observe the same effect. In most experiments conducted in this study no significant change in $CaCO_3$ crystal morphology was observed. Several relatively high acid concentration experiments possibly showed the formation of aragonite crystals, normally only observed at high temperatures. DLS and SEM results showed that silica nanoparticles increased the formation of $CaCO_3$ precipitation and that many smaller crystals formed around the silica nanoparticles.

The second part of the work was dedicated to investigate the effect of a biofilm on the formation of calcium carbonate scale. The involvement of (bacterial) extracellular polymeric substances (EPS) in carbonate precipitation was known from earlier studies. Initially acidic polysaccharides are expected to inhibit carbonate precipitation, but EPS decay might result into a highly organized template structure favouring calcium carbonate nucleation and enhanced precipitation of calcium carbonate with functional groups on EPS acting as initial nucleation sites. The developed method using a small-scale dynamic set-up as well as a flow-loop set-up showed that the biofilm consisting of colonies of the bacterium *Thermaerobacter* sp., the fungus *Penicillium citrinum,* and formed EPS dissolve in flow configuration, especially at higher (≥ 50 °C) temperatures, making detailed kinetic investigations impossible. However, the biofilm components seem to develop intense interaction with the ions, nuclei and/or crystals formed during the executed experiments, which could be shown by detailed microscopic studies. Also, it seems that the transformation of the intrinsically formed vaterite morphology to equilibrium calcite morphologies is delayed or hindered.

2 PART I – ORGANIC AND INORGANIC COMPOUNDS

2.1 REACTIVE ORGANIC COMPOUNDS IN SUBSURFACE WATER

Organic compounds show a large diversity in composition and molecular structure and are present in all natural environments. Also, in deep subsurface environments, such as deep fracture waters [1, 2] thermal water springs [3-5], hydrothermal vents [6-8], oil field waters [9-12], and geothermal fluids [13-18], various dissolved organic compounds have been found including aliphatics, aromatics, carboxylic acids, phenols, humic acids, and alcohols.

Carboxylic acids were commonly reported in geothermal fluids used for energy production [16, 18]. They can be released from organic matter-rich deposits [9, 19] into the water or produced by microbially fermentative microorganisms [20]. The most abundantly found carboxylic compounds are the short chain monocarboxylic acid anions with 1-5 C atoms, named formate, acetate, propionate, butyrate, and valerate. The most common dicarboxylic acid anions found in subsurface waters are oxalate, malonate, succinate, and glutarate [21, 22].

The abundance of both mono- and dicarboxylic acid anions was described in great detail for oil-field waters [9-12]. Acetate was described as the most abundant compound followed by, in order of increasing carbon atoms, propionate, butyrate, and valerate. Formate, which only contains one carbon atom did not seem to follow this trend but was also reported in the oil-field waters. Their concentrations seemed to be controlled primarily by the subsurface temperature and age of the host rock. Figure 1 shows three zones with distinct carboxylic acid concentrations. Zone 1 is characterized by low temperatures and low carboxylic acid concentrations. The low concentrations were attributed to microbial degradation of the carboxylic acids. Zone 2 represents initially increasing concentrations with increasing temperatures, which then decline with temperatures above 100°C. The initial increase of concentration was explained by less microbial degradation since microorganisms would not survive within higher temperature conditions. The decrease of carboxylic acid concentrations was attributed to thermal degradation. This is also the main driver for the low concentrations in Zone 3.

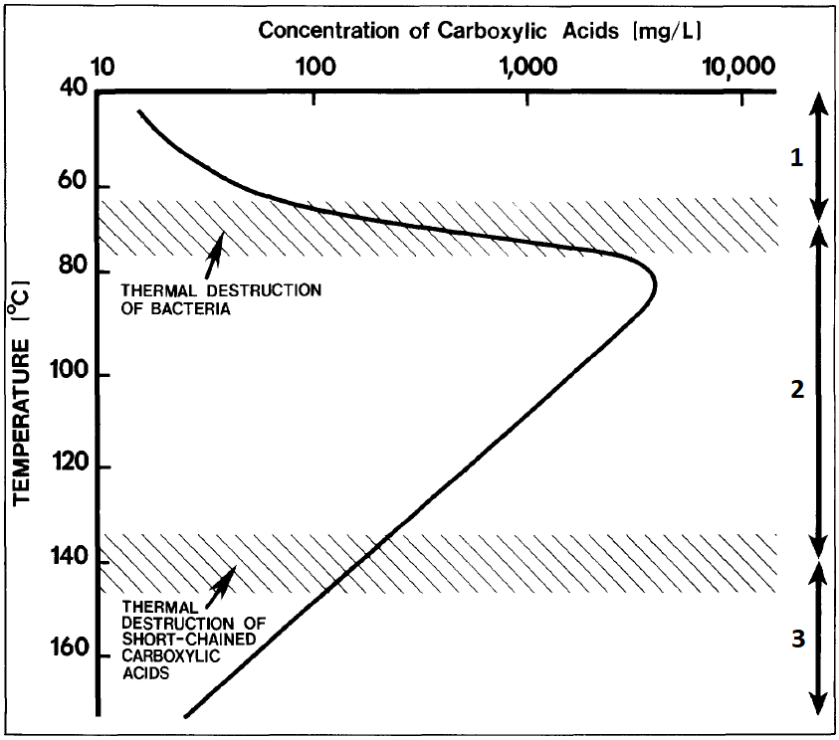

Figure 1: Temperature vs Carboxylic Acid concentration, three zones can be identified. [1]

2.2 POSSIBLE EFFECTS OF ORGANIC COMPOUNDS ON SCALE FORMATION

Several effects of different reactive organic compounds have been investigated. Liu et al. [23] found that the absorption of large organic compounds containing a high density of carboxylate functional groups increased $CaCO_3$ crystal size and decreased nucleation time. It is suggested that high density carboxylate functional groups may enhance surface crystallization by attracting the calcium ions. Surdam et al. [22] proposed the possibility of the carboxylic acid anions forming salts with calcium ions. These salts have a higher solubility than $CaCO_3$, which will keep calcium in solution and reduce scale formation. Lebron et al. [24, 25] investigated the effect of organic ligands and the partial CO_2 pressure (p_{CO2}) on calcite scale formation. It was found that the calcite precipitation rate at certain saturation ratios (SR) and at p_{CO2} of 5 and 10 kPa decreased when the bulk concentration of dissolved organic carbon (DOC) increased. The DOC concentration needed to be increased to cause an equal reaction at higher P_{CO2}. It was proposed to evaluate the quantification of the reduction of calcite precipitation due to DOC at different p_{CO2}. Kitano et al. [26] investigated the effect of organic compounds on the morphology of $CaCO_3$ crystallisation. It was found that the compounds citrate, malate, pyruvate, glycylglycine and glycogen greatly reduce the total $CaCO_3$ precipitation and favor the formation of calcite above the other morphologies. Other tested compounds were found to have a moderate effect on the rate of precipitation and mixed effects on the resulting morphology. Glutamate caused vaterite and calcite to precipitate; lactate, chondroitin sulfate, succinate and arginine favored calcite formation; glycine and serine favored vaterite and aragonite precipitation; and taurine caused aragonite to precipitate. Galactose, dextrose, alanine and acetate were found to have little effect on the precipitation rate and morphology. Wada et al. [27] found that carboxylic acids interact with the crystal surface of $CaCO_3$. The carboxylic acids distort the crystals morphology by adsorbing to the surface. It was also found that carboxylic acids adsorbed on aragonite nuclei at the start of the crystallization process and inhibited their growth. Wada et al. [8] also found that carboxylic acids are effective growth modifiers, but have no influence on the nucleation of $CaCO_3$. This phenomenon can be explained by the fact that carboxylic acids have a stronger affinity for $CaCO_3$ than for free Ca^{2+} ions.

2.3 CARBOXYLIC ACIDS USED IN EXPERIMENTS

The organic compounds chosen for investigation are all carboxylic acids as these are the most common organic species in subsurface water and have been studied before. [22, 26]. The carboxylic acids chosen are acetic acid (CH_3COOH), malonic acid ($CH_2(COOH)_2$), benzoic acid (C_6H_5COOH) and citric acid ($C_6H_8O_7$). Acetic, malonic and citric acid have respectively one, two and three carboxylic acid groups as can be seen in Figure 2. Using these acids, the effect of more carboxylic acid groups in the acid molecule can be investigated. To investigate the effect of other groups attached to the carboxylic acid, benzoic acid has been chosen as it has an aromatic ring attached to the acid group. Table 1 shows the maximum acid concentration observed in subsurface water. Concentrations chosen in this research are based on these values and are further discussed below.

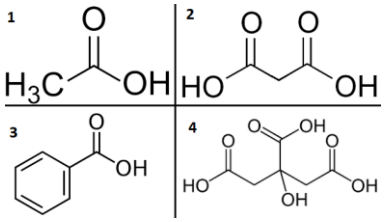

Figure 2: (1) Acetic Acid, (2) Malonic Acid, (3) Benzoic Acid, (4) Citric Acid

Table 1: Maximum reported acid concentrations in subsurface waters [2]

Carboxylic acid	Maximum reported concentration (mmol/L)
Acetic acid	170
Malonic acid	24
Benzoic acid	0.033
Citric acid	0.021

2.3.1 Set-up to study Bulk Precipitation with Dynamic Light Scattering (DLS)

In Figure 3 the set-up used for determining the bulk precipitation is shown. In this set-up, both 100 ml of $NaHCO_3$ solution and 100 ml of $CaCl_2$ solution are mixed in a beaker at the start of the measurement. The reaction that takes place after mixing is:

$$NaHCO_3 + CaCl_2 \xrightarrow{H_2O} CaCO_3\downarrow + NaCl + HCl.$$

For the detection of the $CaCO_3$ particles, a DLS-set-up based on the 3D cross correlation geometry as developed by LS Instruments. The Nanolab 3D consists of a laser that emits light at a wavelength of 685 nm. This light is directed at the dispersion through a polarization maintaining optical fiber. The scattered light by the particles at 90° with respect to the incident beam is collected by a second optical fiber. This specific set-up is based on two simultaneous light scattering experiments performed on the same sample by two beams and two detectors. The signals seen by the detectors are cross-correlated, which enables the DLS to measure flowing samples [28, 29]. An Ismatec pump (Reglo Digital ISM832) pumps the mixed solution through a flow-cuvette in the DLS and back into the beaker creating a loop. By using this flow loop the formation of particles over time can be studied. The solutions are prepared by dissolving (A) $NaHCO_3$ and (B) $CaCl_2$ in 1 or 2 liters of Milli-Q water. The nominal values are shown in
Table 2. Mixing both solutions 1:1 result in a solution with the saturation ratio given in Table 1. Before use in the experiments all solutions are filtered through a 0.22 µm membrane filter to minimize unwanted particles that can influence the DLS measurement. Between experiments the set-up is cleaned with a HCl solution and a control measurement using Milli-Q water was performed.

Table 2: Brine compositions

Saturation Ratio	$NaHCO_3$ (mol/L)	$CaCl_2$ (mol/L)
5	0.005	0.005
9	0.0075	0.0075
15	0.01	0.01
50	0.0235	0.0235

*For comparison the $K_{sp} = 4,7E^{-9}$ which corresponds to a concentration of 0,00069 mol/L of $NaHCO_3$ and $CaCl_2$.

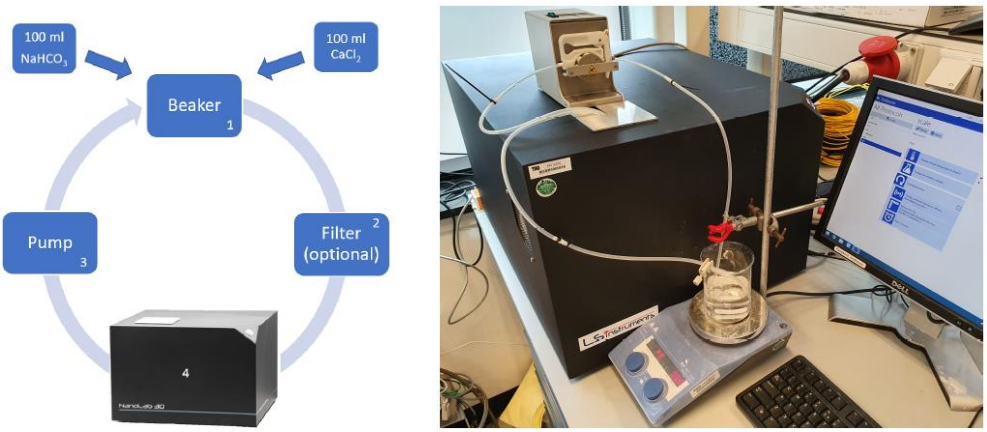

Figure 3: Schematic drawing and picture of the DLS Flow set-up.

To study the effects of the carboxylic acids on the formation of $CaCO_3$ precipitate various amounts of these acids were added to the $NaHCO_3$ solutions as shown in Table 3. After addition of the acids the pH was brought back to the level it was before the addition (approximately 8.7) with a 1M NaOH solution. This has been done to avoid the effect of pH on the formation of precipitation and focus on the carboxylic acids.

Table 3: Carboxylic acid concentrations.

Saturation Ratio	Acetic Acid (mmol/L)	Malonic Acid (mmol/L)	Benzoic Acid (mmol/L)	Citric Acid (mmol/L)
9	0.9 9.0	0.25 0.5 1.0		
15	0.9 4.5 9.0 18.0 45.0	0.25 0.5 0.75 1.0	0.4 2.0 4.0	0.05 0.1 0.25
50	0.9 4.5 9.0 18.0 45.0 90.0	0.25 0.5 1.0 5.0 10.0	4.0 8.0 12.0 16.0	0.1 0.25 2.5

2.3.2 Seeded growth experiments

To improve the DLS experiments and to investigate the effect of particulates that are present in the solution beforehand, several experiments have been conducted using silica nanoparticles (SiO_2). These particles have been added to the $NaHCO_3$ solution before the start of the experiment. The

nanoparticles used in these experiments was Levasil CC301, a colloidal silica suspension with 28.1% solids by weight and a nominal particle size of 7 nm. These experiments have been conducted at a saturation ratio (SR) 5 to minimize homogeneous nucleation. The saturation ratio, which is an indication of the tendency of the crystallisation to occur, is defined by the following formula:

$$SR = \frac{Me * An}{K_{sp}}$$

Where M_e is the ion activity of Mg^{2+}, Ca^{2+}, Sr^{2+} or Ba^{2+}, A_n is the ion activity of CO_3^{2-} or SO_4^{2-} and K_{sp} is the solubility product. The formation of scale can occur when the saturation ratio is larger than 1. The pH at the start of the experiments is set at ~9.5 due to the fact that at this low supersaturation no precipitation occurs at pH 8.7 as used in the before mentioned experiments.

2.3.3 Morphology

To investigate the effect of the carboxylic acids on the morphology of the calcium carbonate crystals, samples have been taken at the end of each experiment for Scanning Electron Microscopy (SEM). These samples were centrifuged at 1200 rpm for 15 minutes to concentrate the particles. The liquid layer has been removed and the particles have been washed with Milli-Q water to reduce the high concentrations of still dissolved salts in the solution. After this wash step the samples have been centrifuged again at 1200 rpm for 15 minutes. No dissolution of scale particles was observed. A portion of the particles have been removed with a pipette and deposited on a sample holder. These samples were dried overnight at room temperature after which SEM measurements were conducted using a Phenom World and a FEI Quanta 600.

2.4 RESULTS AND DISCUSSION

To investigate the effect of the four carboxylic acids on the $CaCO_3$ precipitation a basis of comparison had to be established. To generate this basis several precipitation experiments have been conducted where no acids were added into the mixture at SR's of 50, 15, 9 and 5.

2.4.1 Precipitation

In Figure 4 the scaled count rates of the above-mentioned experiments are shown over time. At SR50, SR15 and SR9 an increase in count rate over time is observed, indicating the formation of $CaCO_3$. At SR5 no precipitation occurred during the 4 hours run-time of the experiment and so no increase in count rate is observed. As the saturation ratio decreases, an increase in induction time, indicated by the onset of the increase in scaled count rate, is observed until no precipitation occurs anymore during the experiment. The maximum scaled count rate decreases as the saturation ratio decreases, indicating that less precipitation is formed as the saturation ratio decreases.

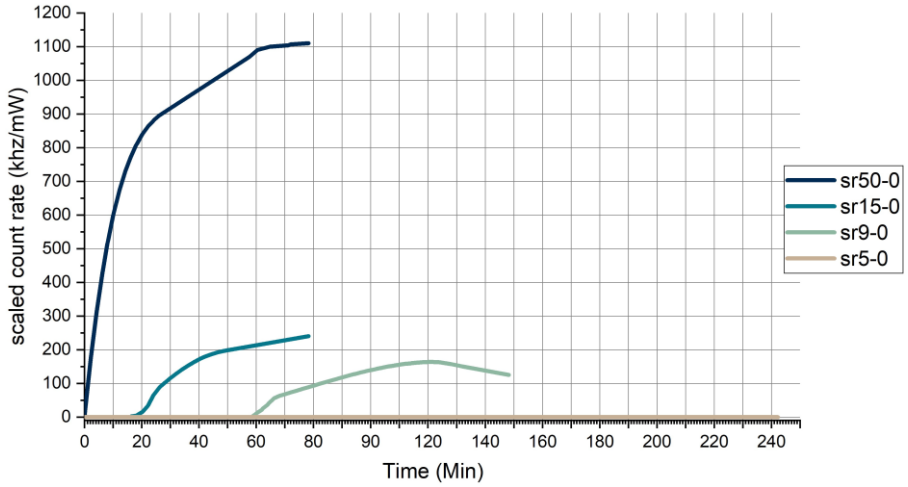

Figure 4: Scaled count rate of CaCO3 precipitation at SR50, SR15, SR9, SR5.

In Figure 5 the mean particle radius over time of the $CaCO_3$ crystals at SR50, SR15 and SR9 is shown. At all three saturation ratios a steep increase in particle radius is observed at the start of precipitation after which the radius stabilizes at around 500 nm. To verify the measured particle radius SEM samples were taken. In these SEM images a large variation in particle size is observed. These particles range from below 100 nm to above 10 µm. Due to this large variation in particles size the radius measured by the DLS is influenced. A few large particles can overshadow many smaller particles. Another problem is that the particle size limit of the DLS is 10 µm, any larger particles will distort the measurement and will give results that are not representative. As this large variation in particle size is observed in most experiments conducted in this research the particle radius measured by the DLS is not used for further analysis. Nevertheless, this method allows us to study important aspect of homogeneous nucleation like induction time and relative amounts of precipitate formed by using the scaled count rate.

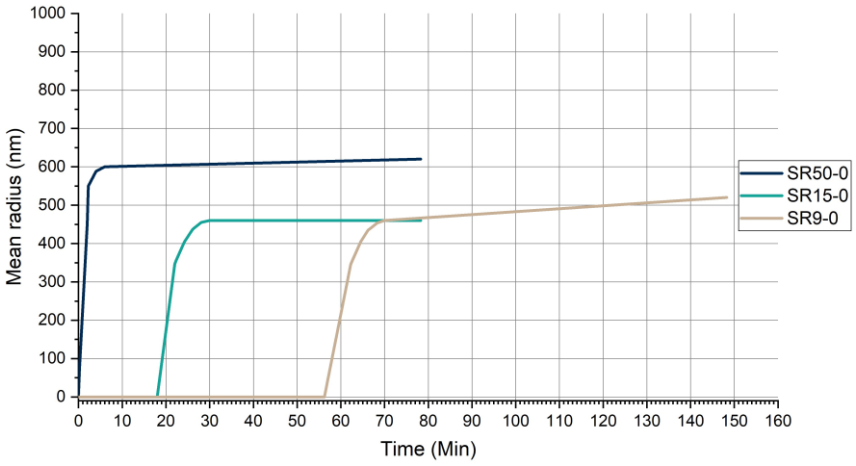

Figure 5: Mean Particle Radius of CaCO3 precipitation at SR50, SR15, SR9, SR5.

2.4.2 Reproducibility

To investigate the reproducibility of the experiments several identical experiments with no addition of acid have been conducted at SR50 and SR15, the latter can be seen in Figure 6. These experiments show no measurable variance in induction time at SR50 as it is very short. The results of SR15 on the other hand show an induction time that ranges from 6 to 18 minutes indicating that other factors in the set-up have an influence on the precipitation.

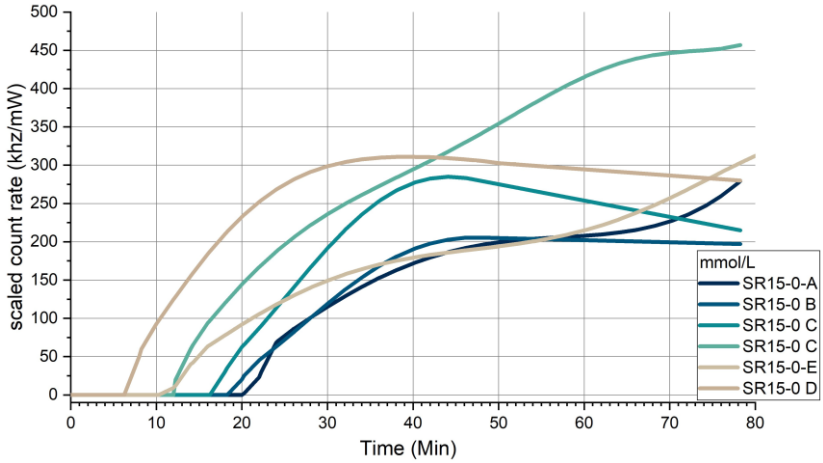

Figure 6: Scaled count rate of $CaCO_3$ precipitation at SR15, six identical experiments were conducted with no addition of any acid.

One of the factors influencing the variation of induction time might be the storage time of the used $NaHCO_3$ and $CaCl_2$ solutions. The composition and pH of these solutions might change a little over time by reacting with the surrounding air resulting in changes in the Saturation Ratio. Another factor might be that the set-up is an open system, particles occurring in the air might settle in the beaker resulting in heterogeneous precipitation to occur. Also, even though the system is cleaned (HCl) there might be some seed crystals remaining. Due to this 12-minute variation in induction time at low saturation ratio's, it can be concluded that changes in induction time, that fall within this variation, might not be caused by the addition of the carboxylic-acids and are a result of the set-up used.

2.4.3 Morphology

To find a basis of comparison for the $CaCO_3$ morphology, samples have been taken at the end of the experiments. These samples have been analyzed with SEM. As well as the large variation in particle size, several morphologies of $CaCO_3$ can be observed in the SEM images.
The two most abundant morphologies are cubic/rhomboetric crystals and spherical/hexagonal crystals which correspond to calcite and vaterite respectively (see Figure 7 below).

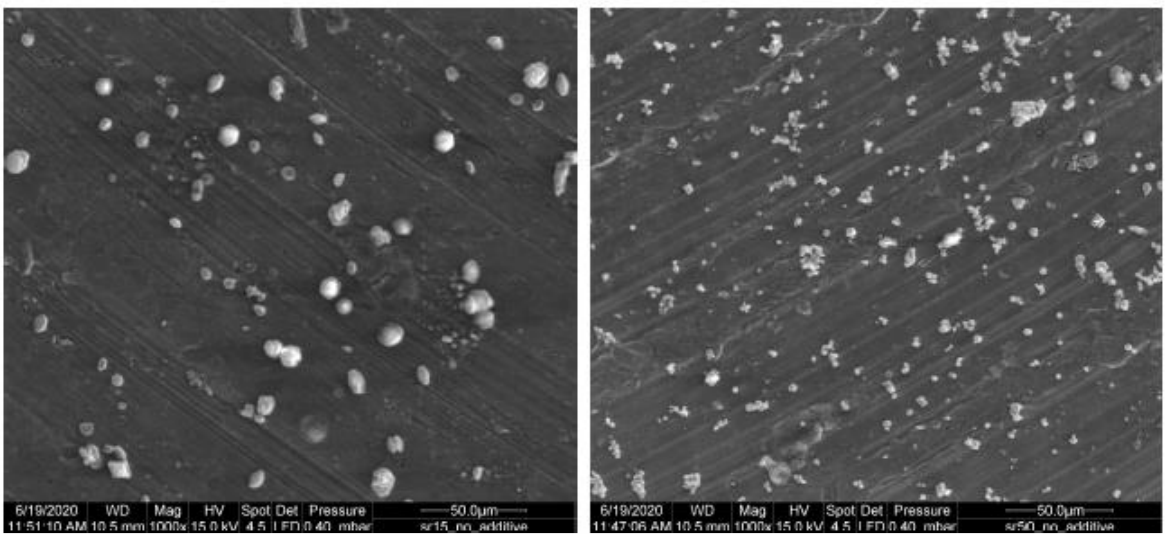

Figure 7: SEM of CaCO3 crystals, SR15-0 and of CaCO3 crystals, SR50-0 (1000x).

2.5 INFLUENCE OF CARBOXYLIC ACIDS ON SCALING

2.5.1 SR50

To determine the influence of acetic acid, malonic acid, benzoic acid and citric acid at SR50 several experiments have been conducted in which increasing concentrations of acid have been added to the mixture of $NaHCO_3$ and $CaCl_2$. In Figure 8 the effect of acetic acid at SR50 is shown. In all experiments the precipitation starts instantaneously and no effect on the induction time is observed as shown by the onset of the count rate. As the concentration of acetic acid is increased, a decrease in total precipitation is observed as seen by the decrease in maximum count rate. At an acetic acid concentration of 18 mmol/L this drop was first clearly observed. At a concentration of 0.9 and 4.5 mmol/L acetic acid a drop on count rate is observed at the end of the experiment. However, this drop is caused by sedimentation in the flow cuvette which decreases the measurable particle concentration in the solution which in turn results in a lower count rate.

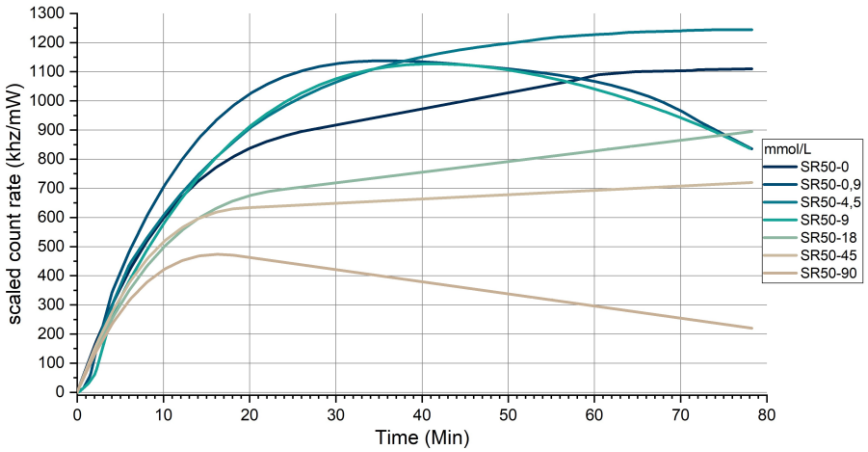

Figure 8: Scaled count rate of $CaCO_3$ precipitation at SR50 after addition of acetic acid.

In Figure 9 the effect of malonic acid at SR50 is shown. Again, no difference in induction time was observed. A decrease in maximum count rate was observed as the acid concentration increased. At a malonic acid concentration of 0.5 mmol/L this drop was first clearly observed. This decrease starts at a much lower acid concentration in comparison with acetic acid (0.5 mmol vs 18 mmol). Above 0.5 mmol acid concentration sedimentation is also observed in the cuvette and is shown as a drop in the scaled count rate in Figure 9. This may be attributed to the presence of bigger particles in these experiments compared to experiments at 0 and 0.25 mmol/L malonic acid.

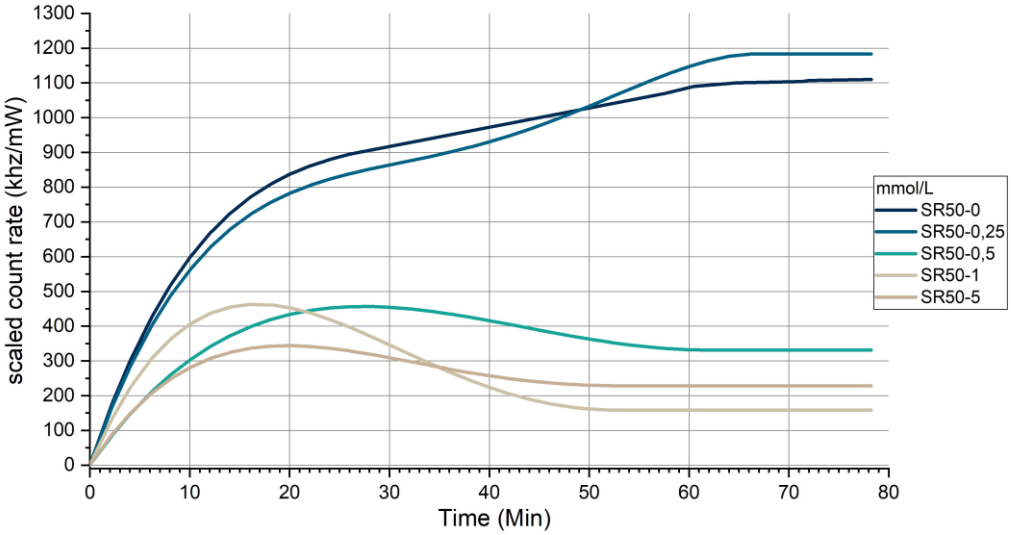

Figure 9: Scaled count rate of $CaCO_3$ precipitation at SR50 after addition of malonic acid.

The effect of citric acid at SR50 is shown in Figure 10. For the first time an increase in induction time, indicated by the onset of the count rate, is observed as acid concentration increases. Again, a decrease of the maximum count rate is observed with increasing acid concentrations. This decrease is observed at even lower acid concentrations in comparison to acetic and malonic acid (0.1 vs 0.5 mmol/L). At 2.5 mmol/L citric acid concentration no precipitation was observed during the experiment.

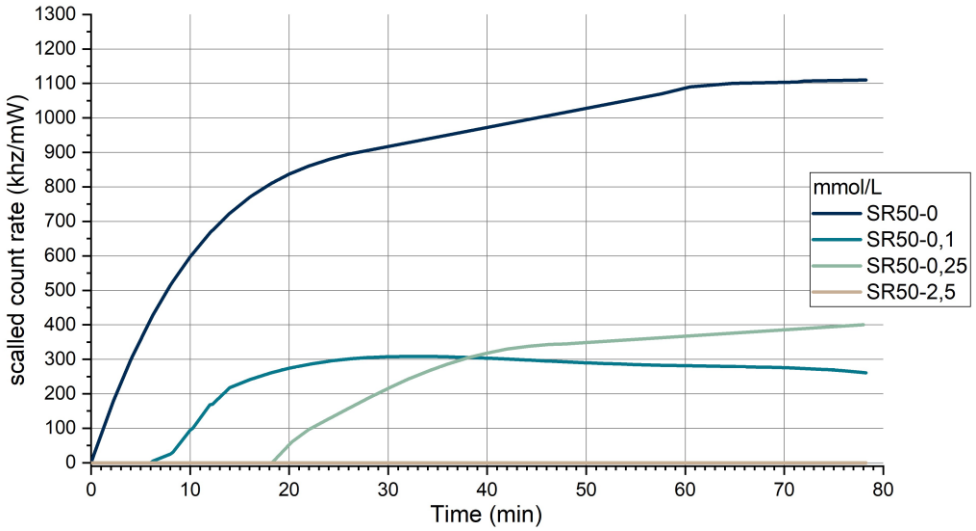

Figure 10: Scaled count rate of $CaCO_3$ precipitation at SR50 after addition of citric acid.

In Figure 11 the effect of benzoic acid at SR50 is shown. A decrease in maximum count rate is observed and no increase in induction time is observed as acid concentration increases. At 12 mmol/L benzoic acid concentration and above no precipitation was observed during the experiment. At a concentration of 8 mmol/L benzoic acid sedimentation occurs in the cuvette as indicated by the drop on count rate after reaching a maximum.

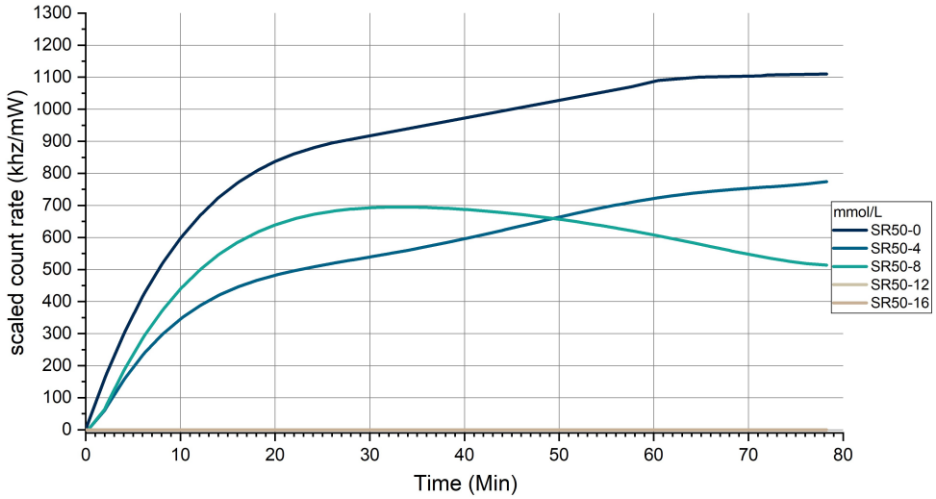

Figure 11: Scaled count rate of $CaCO_3$ precipitation at SR50 after addition of benzoic acid.

2.5.2 SR15

The effect of acetic acid at SR15 is shown in Figure 12. Already without addition of acid, the count rate is considerably lower than at SR50. In contrast to SR50, an increase in induction time is observed as acid concentration increases. A decrease in maximum count rate is observed as well. The induction time is increased from 16 minutes at 0 mmol/L to more than 130 minutes at 9 mmol/L and above. As induction time increases total precipitation decreases. In comparison to SR50 the onset of the decrease in total precipitation is observed at lower acid concentrations.

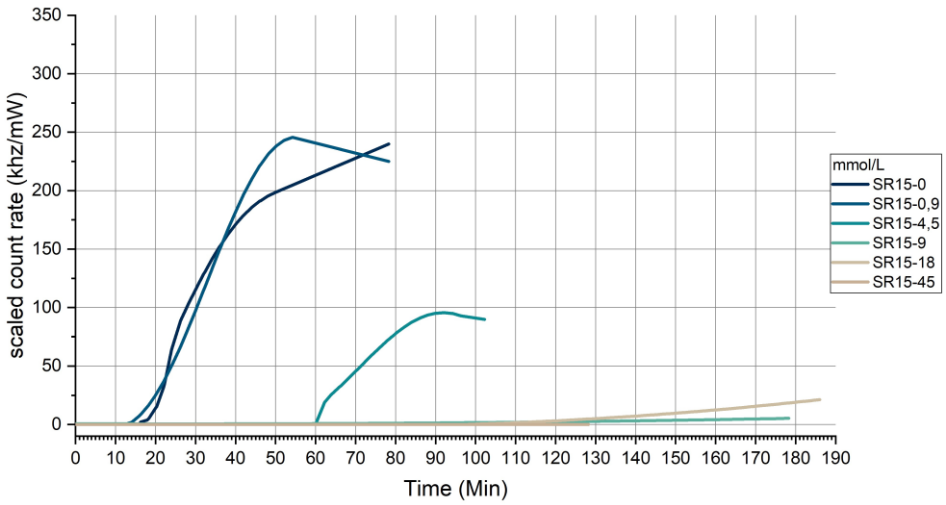

Figure 12: Scaled count rate of $CaCO_3$ precipitation at SR15 after addition of acetic acid.

Figure 13 shows the effect of malonic acid at SR15. An increase in induction time and a decrease in maximum count rate is observed as acid concentration increases. The induction is increased from 16 minutes at 0 mmol/L to more than 50 minutes at 0.75 mmol/L and above. In comparison to SR50 the effect of Malonic acid is larger at lower concentrations.

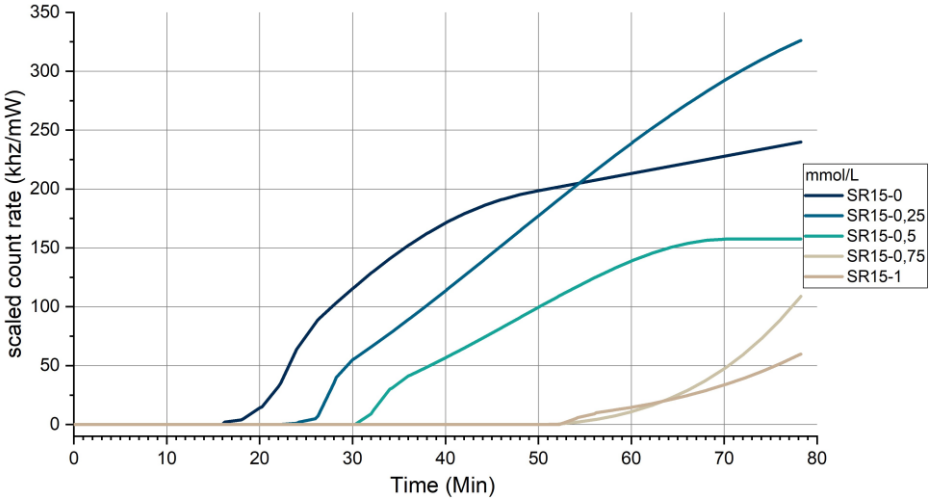

Figure 13: Scaled count rate of $CaCO_3$ precipitation at SR15 after addition of malonic acid.

In Figure 14 the effect of citric acid at SR15 is shown. Both an increase in induction time and a decrease in total precipitation is observed. The induction time is increased from 16 minutes at 0 mmol/L to more than 120 minutes at 0.25 mmol acid concentration. In comparison to SR50 the effect of Citric acid is larger at lower concentrations. In comparison to the acetic and malonic acid the effect is more pronounced and starts at lower acid concentrations.

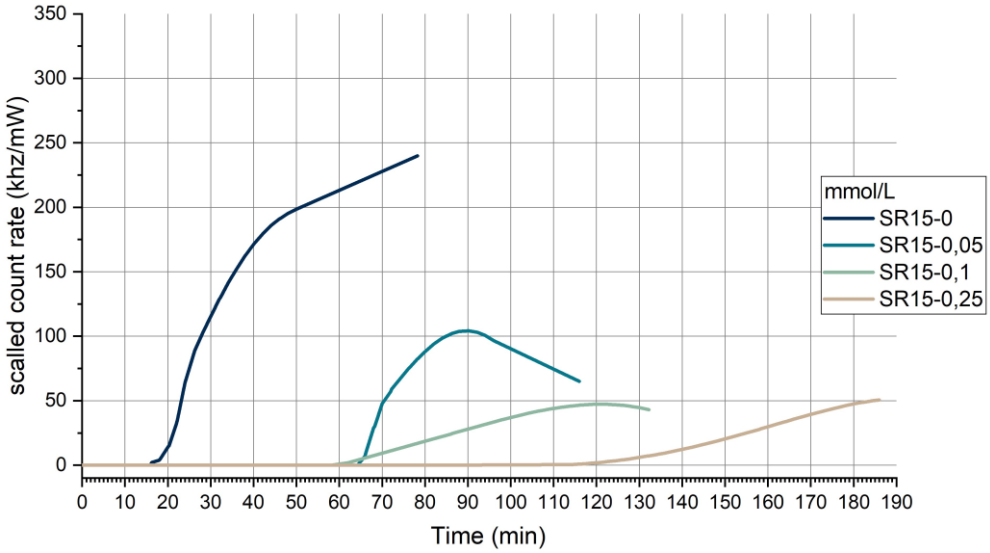

Figure 14: Scaled count rate of $CaCO_3$ precipitation at SR15 after addition of citric acid.

Figure 15 shows the effect of benzoic acid at SR15. In general, the same decrease in total precipitation and increase in induction time as the other acids is seen. However, the addition of 0.4 mmol/L benzoic acid seems to show a different trend as more precipitation seems to be formed first. As discussed above, the induction time at SR15 varies between 6 and 18 minutes. The measurement of 0.4 mmol/L benzoic acid fits within this variation indicating no significant effect on the $CaCO_3$ precipitation compared to no addition of benzoic acid.

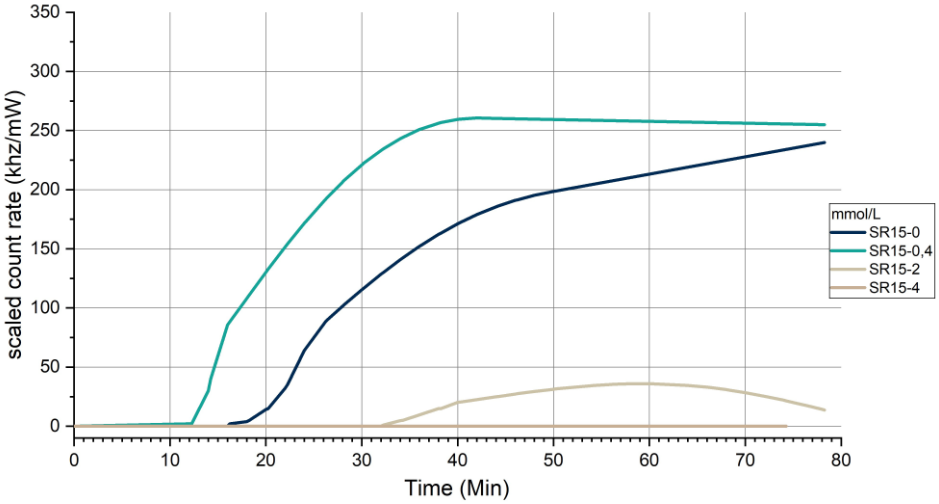

Figure 15: Scaled count rate of $CaCO_3$ precipitation at SR15 after addition of benzoic acid.

2.5.3 SR9

To determine the influence of acetic acid, malonic acid at SR9 several experiments have been conducted in which increasing concentrations of acid have been added to the mixture of $NaHCO_3$ and $CaCl_2$. The effect of acetic acid at SR9 is shown in Figure 16. An increase in induction time and a decrease maximum count rate is observed as acid concentration rises. When compared to SR50 and SR15 these effects are larger at lower acetic acid concentrations. At a concentration of 9 mmol/L acid no precipitation occurs during the experiment. After reaching a maximum, a drop in the count rate is observed at a concentration of 0 and 0.9 mmol/L acetic acid. This drop is caused by sedimentation in the cuvette.

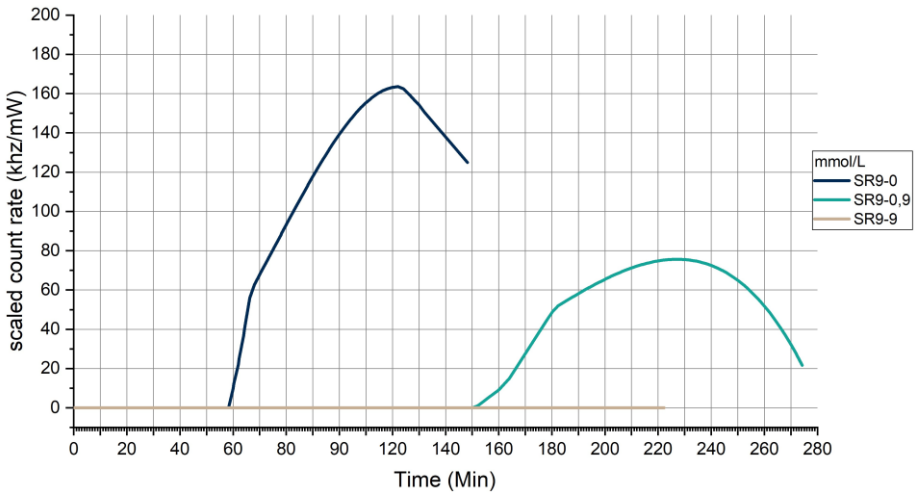

Figure 16: Scaled count rate of $CaCO_3$ precipitation at SR9 after addition of acetic acid.

Figure 17 shows the effect of malonic acid at SR9. Again, a decrease in maximum count rate is observed on addition of malonic acid. The induction time does not seem to increase significantly up to a concentration of 0.5 mmol/L. At a concentration of 1 mmol/L malonic acid no precipitation occurs during the experiment. The drop in the count rate at 0 mmol/L malonic acid after reaching a maximum is caused by sedimentation in the cuvette. When comparing these results with SR50 and SR15 the effects on induction time and relative precipitation is larger at lower malonic acid concentrations.

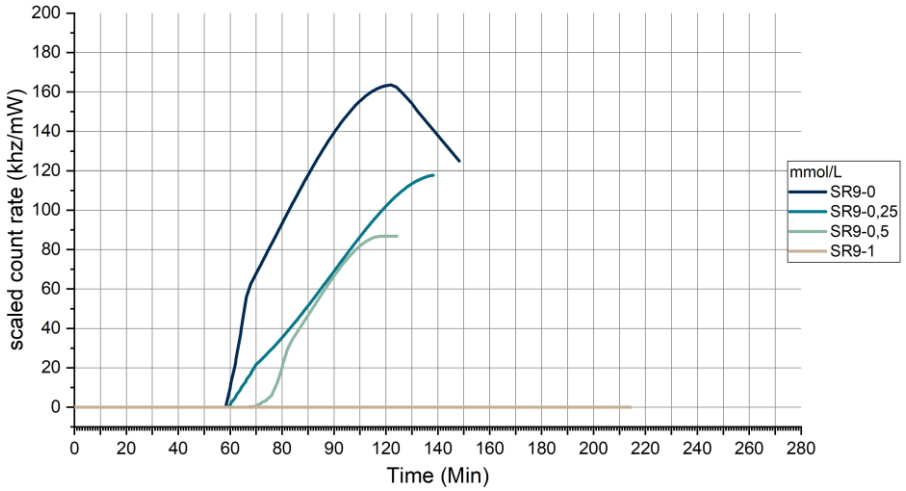

Figure 17: Scaled count rate of $CaCO_3$ precipitation at SR9 after addition of malonic acid.

2.6 COMPARISON BETWEEN CARBOXYLIC ACIDS

The downward trend in maximum count rate observed after addition of the acids studied, indicates that these acids have an inhibitory effect on the homogeneous nucleation of $CaCO_3$ at SR50. This is in contradiction to Wada et al. [8]. Generally, it is observed that an increase in concentration of acetic acid, malonic acid, benzoic acid and citric acid results in less $CaCO_3$ precipitating. When comparing the acetic, malonic and citric acid results it is shown that less acid concentration is needed to reduce the $CaCO_3$ precipitation as the number of carboxylic acid groups increase. The inhibiting effect of the acids observed at SR50 is also observed at SR15 but to a higher degree. Both a decrease in maximum count rate and an increase in induction time is observed after addition of acetic acid, malonic acid, benzoic acid and citric acid. When comparing the SR15 results to SR50, lower acid concentrations are needed to have a significant effect on the precipitation. This suggests that as saturation ratio decreases the effect of the carboxylic acids increases. The downward trend of maximum count rate observed at SR50 and SR15 is also observed at SR9 for acetic and malonic acid but at an even higher degree.

2.7 INFLUENCE OF CARBOXYLIC ACIDS ON $CaCO_3$ MORPHOLOGY

Several studies have shown that the polymorphism of $CaCO_3$ mainly depends on temperature [30, 31]. To study if the presence of acetic acid, malonic acid, benzoic acid and citric acid has an effect on the morphology of the $CaCO_3$ crystals samples were taken after the DLS experiments and were analysed by SEM. In figure 18 the four different morphology's that were observed in the $CaCO_3$ samples are shown. Cubic crystals correspond with calcite, both spherical/hexagonal and flower like crystals correspond with vaterite and needle crystals correspond with aragonite.

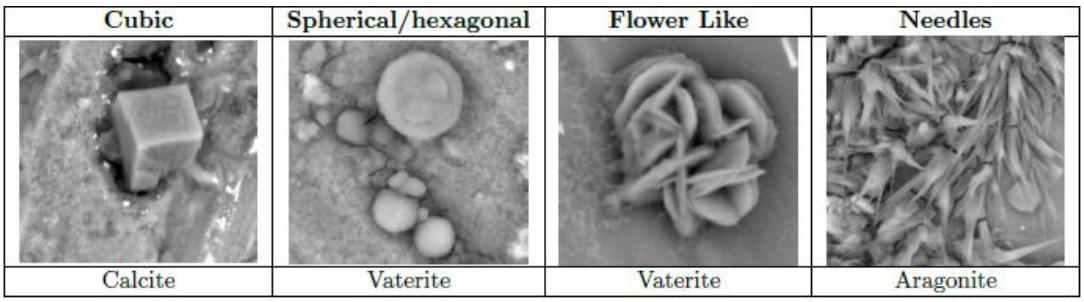

Figure 18: Observed morphology's in CaCO3 samples: cubic/rhombic, spherical/hexagonal, flower like and needles .

In most experiments the carboxylic acids had no observed effect on the morphology of the crystals. Cubic, spherical/hexagonal and flower like crystals were observed in most samples and in a large variation of sizes. The distribution of particles is so chaotic that the distortion of the crystals morphology as reported by Wada et al. [27] cannot be observed using this method. Only samples showing new morphologies will be discussed below and are shown in Table 4.

Table 4: Sample with changes in morphology.

# *	Sample Name	Morphology's
74	SR9-no additive	Cubic and Needles
68	SR9-0,9mmol/L acetic acid	Cubic, spherical and needles
27	SR15-50°C	Cubic and needles
59	SR50-50°C	Cubic and needles
42	SR50-45mmol/L acetic acid	Cubic, spherical, flower like and needles
43	SR50-5mmol/L malonic acid	Cubic, spherical, flower like and needles

In both samples of 50°C needle crystals were observed corresponding with aragonite besides calcite and are shown in Figure 19. This is in agreement with literature [32, 33] as the formation of aragonite is only observed at higher temperatures. Crystal size ranged from 1 µm to more than 10 µm. Samples of SR9 both with and without the addition of acid showed small crystals that had needle like characteristics and suggested the formation of aragonite which was unexpected.

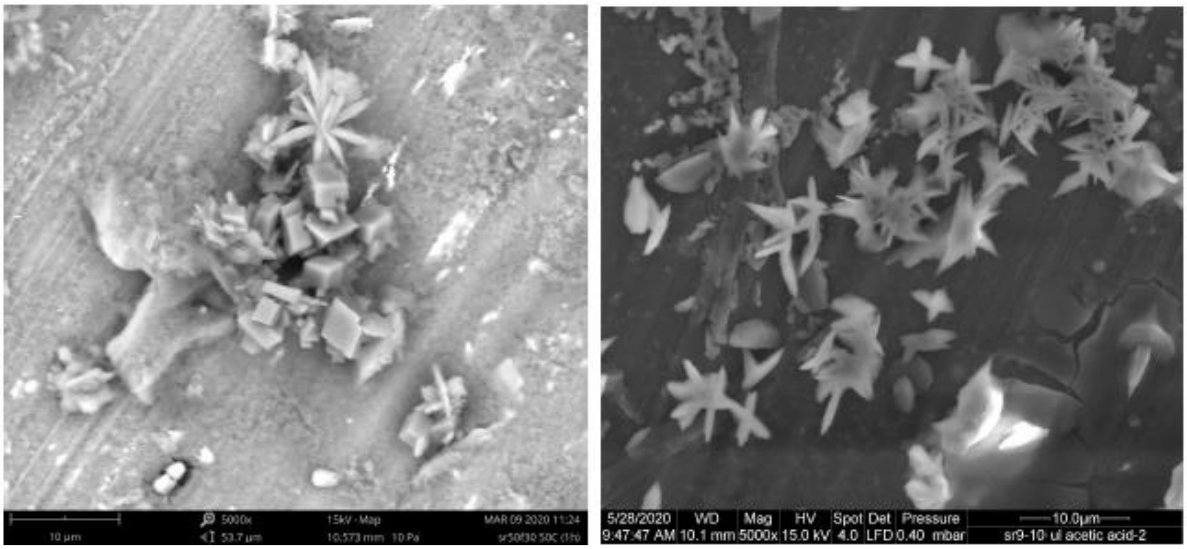

Figure 19: SEM of $CaCO_3$ crystals, SR50-50°C (5000x) and of $CaCO_3$ crystals, SR9-0,9 mmol/L acetic acid (5000x).

Two samples of SR50, one with 5 mmol/L malonic acid and the other with 45 mmol/L acetic acid added showed needle like crystals suggesting the formation of aragonite (Figure 20). Both samples have relatively high concentrations of acid added suggesting the possibility that high acid concentrations can change the morphology of $CaCO_3$.

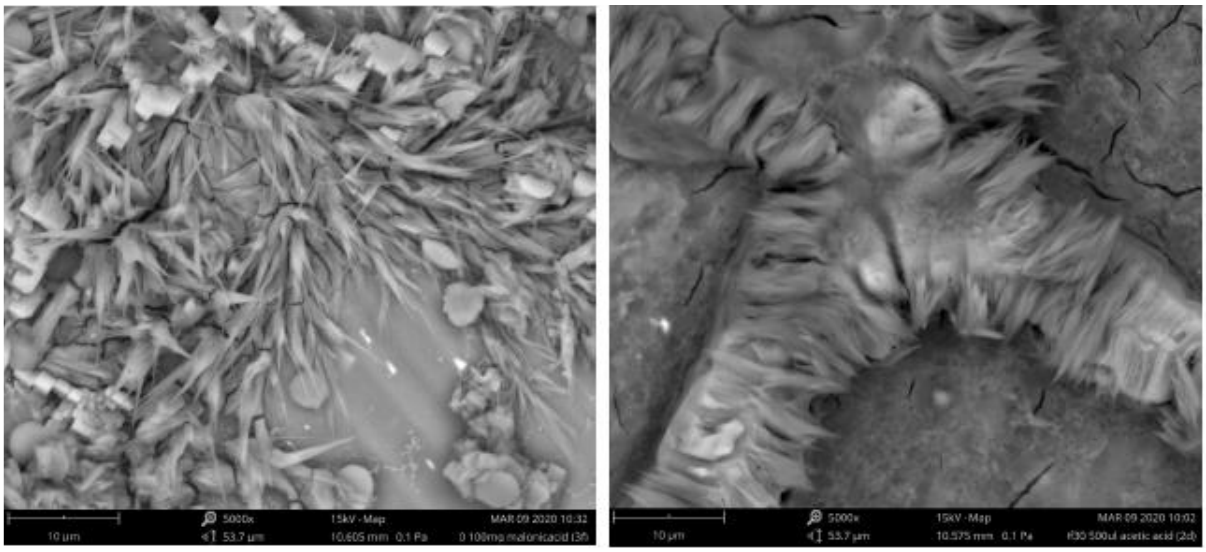

Figure 20: SEM of $CaCO_3$ crystals, SR50 5 mmol/L malonic acid (5000x) and of $CaCO_3$ crystals, SR50 45 mmol/L acetic acid (5000x).

2.8 INFLUENCE OF SILICA NANOPARTICLES AT SR5

To investigate the effect of particulates that are present in the solution beforehand, several experiments have been conducted using silica nanoparticles (SiO_2) see Figure 21. At a pH of 8.7 no precipitation is observed for at least 240 minutes. As no precipitation occurs at pH 8.7, the pH has been set to ~ 9.5 to initiate precipitation at SR5 within reasonable time as can be seen for the brown line in Figure 21. The drop on count rate at 20 minutes is due to sedimentation in the cuvette. The subsequent rise in count rate is produced by flushing the cuvette of the sedimentation and mixing the particles back into the solution. The green line in Figure 21 shows the precipitation in the presence of the SiO_2 seed and shows an increase in maximum count rate in comparison to the experiment without seed. The fluctuation in the count rate is due to sedimentation in the cuvette and subsequently flushing the cuvette. In the presence of the seed particles the effect of sedimentation is smaller. This could indicate that there are fewer large particles that show sedimentation. To investigate this SEM pictures were taken of the particles that were formed in both experiments at pH 9.5.

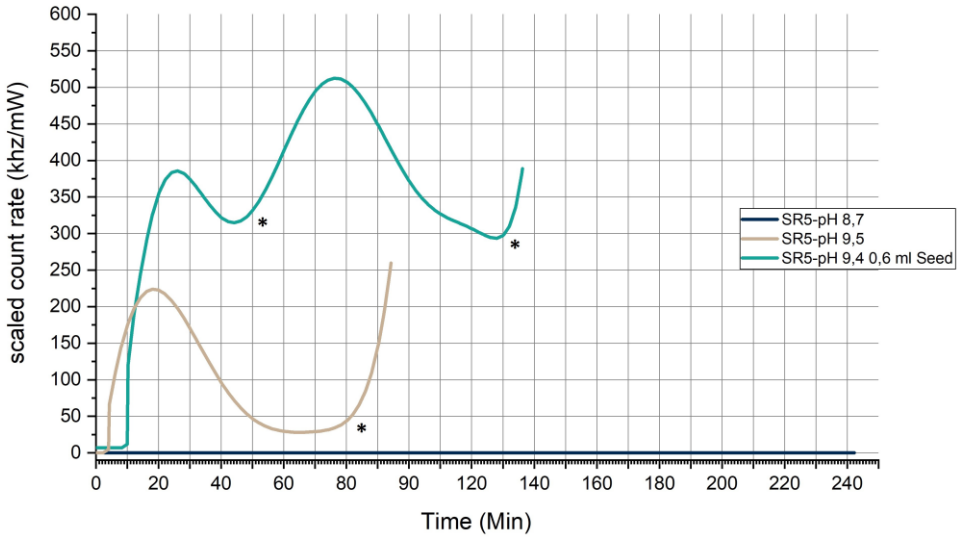

Figure 21: Scaled count rate of $CaCO_3$ precipitation at SR5 after addition of Silica nanoparticles.
*Increase in count rate is caused by flushing the cuvette after sedimentation occurred.

The SEM images shown in Figure 22 are in agreement with the DLS results and show more and smaller particles in the seeded sample. Both samples still contain large calcite and vaterite particles but only the seeded sample shows an abundance of small vaterite particles.

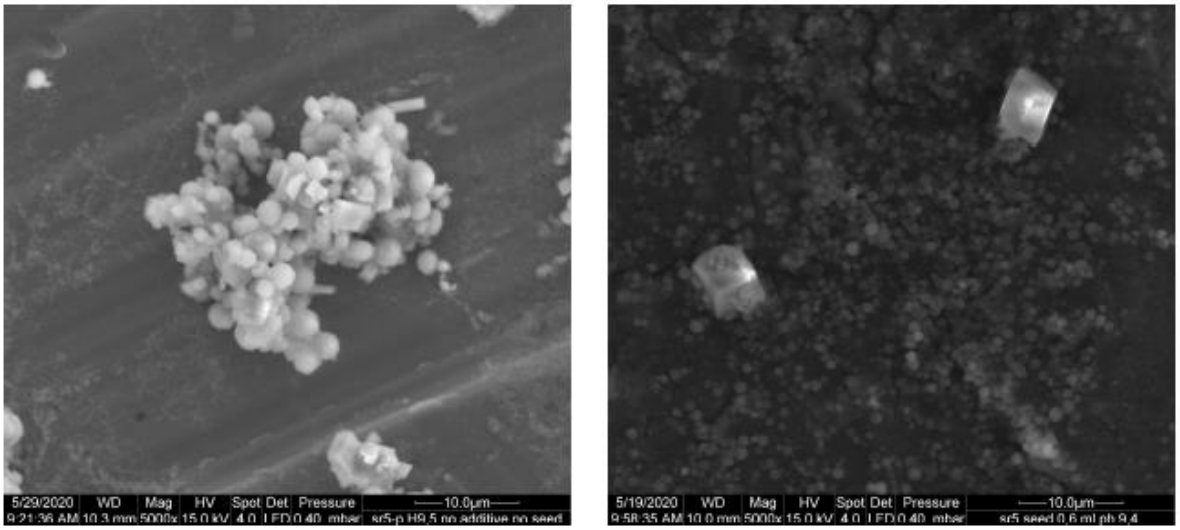

Figure 22: SEM of $CaCO_3$ crystals, SR5-pH 9.5 without seeds (5000x) and of $CaCO_3$ crystals, SR5 pH 9.4 with SiO_2 seeds (5000x).

This experiment proves that it is possible to steer the particle size of scale by addition of seeds. This might be used as a strategy to avoid the deposition of scale crystals.

2.9 CONCLUSION PART I

The goal of this part of the project was to investigate the effect of several common carboxylic acids on the formation of homogeneous calcium carbonate scale. The developed approach using dynamic light scattering (DSL) has proven to be a new method to study important aspects of homogeneous nucleation like induction time and relative amounts of precipitate formed by using the scaled count rate. SEM results in this study showed broad particle size distribution of the formed $CaCO_3$ particles, which makes it impossible for the DLS to measure a representative mean particle size. However, by using the scaled count rate the effects of acetic acid, malonic acid, benzoic acid and citric acid on homogeneous nucleation of $CaCO_3$ could be studied. All carboxylic acids tested in this research had an inhibitory effect on the precipitation of calcium carbonate. Both the induction time and amount of precipitation was influenced by the carboxylic acids. DLS results show as acid concentration increases induction time is increased and total precipitation is reduced. DLS results also show that as carboxylic groups in the acid molecule increase, less acid concentration is needed to observe the same effect. In most experiments conducted in this study no significant change in $CaCO_3$ crystal morphology was observed. Several relatively high acid concentration experiments possibly showed the formation of aragonite crystals, normally only observed at high temperatures. DLS and SEM results showed that silica nanoparticles increased the formation of $CaCO_3$ precipitation and that many smaller crystals formed around the silica nanoparticles.

3 PART II – MECHANISM OF SCALE FORMATION ($CaCO_3$)

Supersaturation of the scaling salts can be triggered/initiated or caused by mixing of different streams of (salt) solutions, but also by pressure changes, especially when gases are dissolved (CO_2) or temperature changes. All this will result in changes of the solubility or even exceeding the solubility limit of dissolved components. Supersaturation does not necessarily result in scale production. Firstly, in the (super)saturated fluids, an intrinsically unstable cluster of atoms, a nucleus is formed – this is called homogeneous nucleation. The atom clusters form small seed crystals triggered by local concentration fluctuations. The seed crystal initiates nuclei formation/growth by further absorbing ions – extending the (crystal) nucleus size. If a nucleus is in an environment of high saturation and has a size greater than the critical size, it will grow, else it will re-dissolve in the solution. The energy for seed growth is driven by a reduction of surface free energy of the nucleus. Crystal growth tend also to occur on a (pre)existing fluid-solid boundary – a surface imperfection. This process is called heterogenous nucleation, the sites are e.g., surface defects, roughness of surfaces etc. (see Figure 23 [34]). Once the initial crystals have started to grow, further scaling will occur.

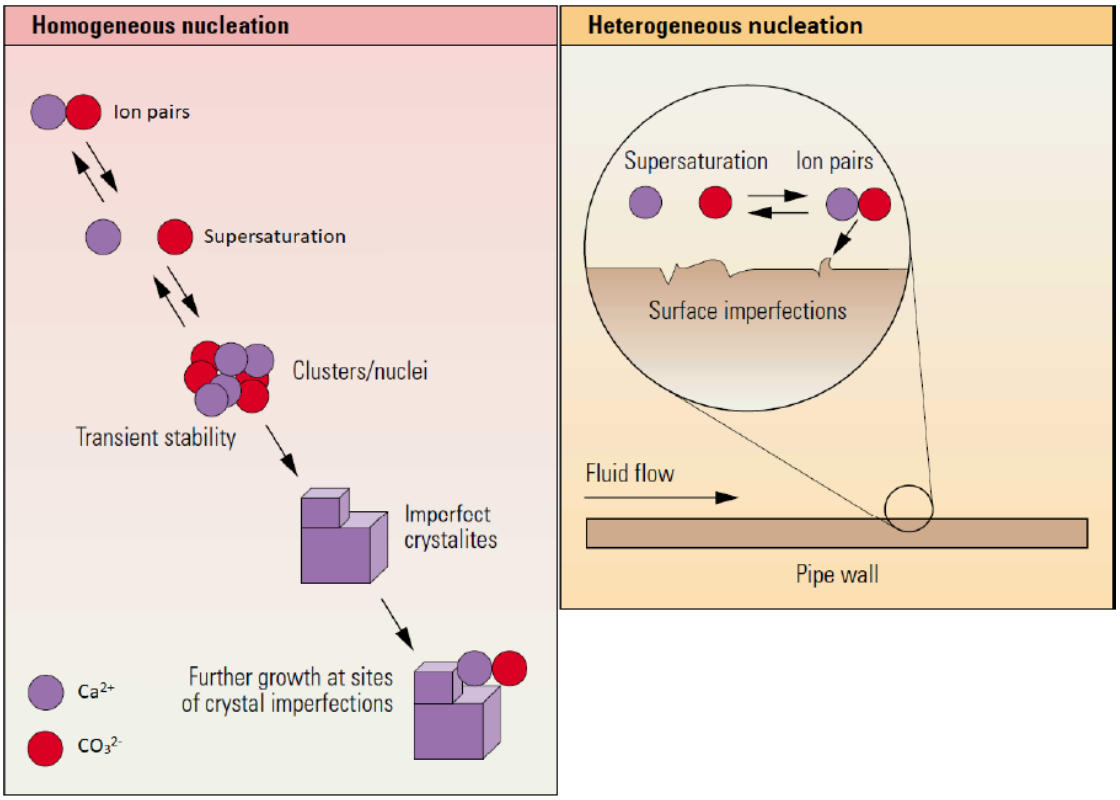

Figure 23: Homogeneous and heterogeneous nucleation [34].

$CaCO_3$ appears to be a nice (model) system for nucleation and crystallization analysis of minerals. This system serves for classical and nonclassical crystallization and has been studied for more than a century. Amorphous calcium carbonate (ACC) is identified as a post-nucleation-stage precursor phase in calcium carbonate mineralization [35]. The chemical composition of ACC is nominally $CaCO_3 \cdot H_2O$ [36]. The ACC structure consists of a calcium-rich nanoscale framework with pores containing water and carbonate ions. The crystallization process occurs in two stages. Firstly, the particles of ACC rapidly dehydrate and crystallize to form individual particles of vaterite. Secondly, the vaterite transforms to calcite via a dissolution and reprecipitation mechanism at low temperatures (< 30 °C) and to aragonite at higher temperatures (≥ 40 °C) [30] see figure 24.

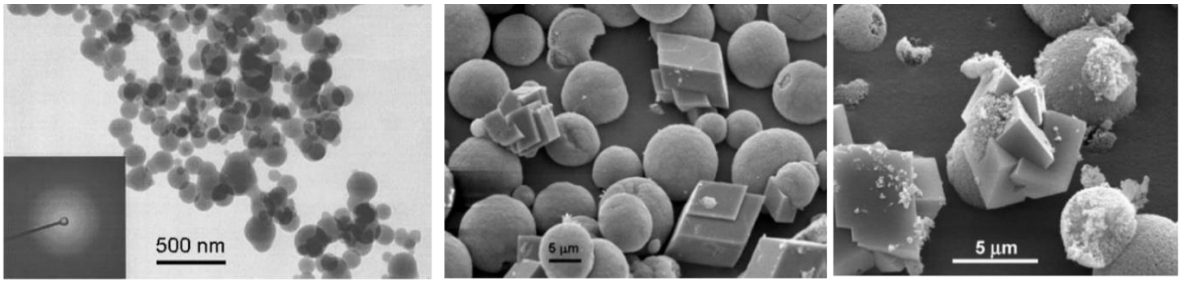

Amorphous $CaCO_3$ (ACC) after 1 min mixing | Transformation to $CaCO_3$ crystals after 5 min mixing | Transformation to $CaCO_3$ vaterite and calcite after 60 min mixing

Figure 24: Mechanism of $CaCO_3$ precipitation [35].

Adding polycarboxylate to the CO_3^{2-} containing solution prior to mixing initially leads to a phase-separated structure (Fig. 25) that is similar to the one observed in the case without polymer (Fig. 24). The amount of additive present during the precipitation plays a decisive role for the further evolution of the precipitate. If the amount of polymer is insufficient to cover the surfaces of the nanoparticles efficiently, dissolution of the primary particles occurs resulting in recrystallization of $CaCO_3$ to crystals of mesoscopic size. Since the polycarboxylates are able to dissolve $CaCO_3$ due to their higher binding strength they will be fully complexed with Ca^{2+}-ions and precipitate. If sufficient organic polymers (e.g., polycarboxylic acid) are added, the nanoparticles are stabilized (against compaction and recrystallization), and then form amorphous precipitates.

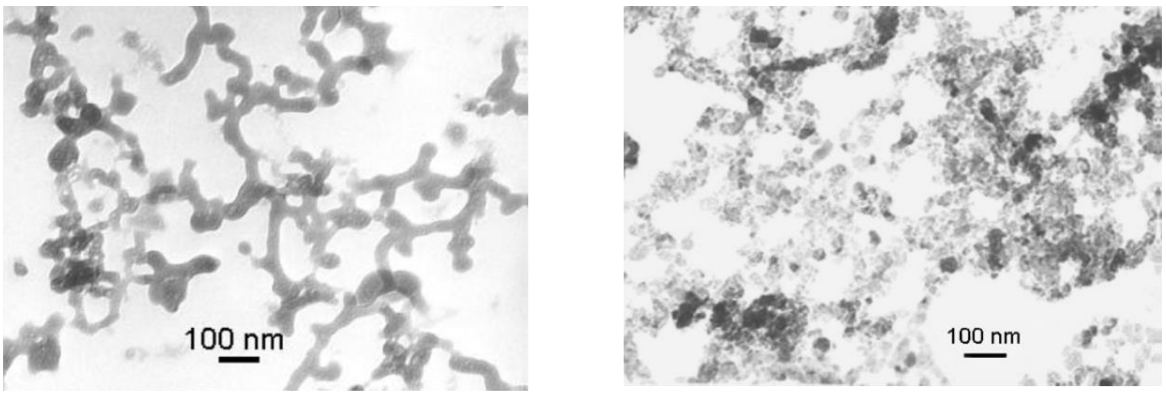

Amorphous $CaCO_3$ (ACC) with polycarboxylate present after 0.1 min mixing | Partially transformation to $CaCO_3$ crystals after 5 min mixing

Figure 25: $CaCO_3$ precipitation in presence of Polycarboxylates [35].

3.1 BIOMINERALIZATION PROCESSES

Biologically controlled precipitation occurs at atomic/molecular-scales where nucleation and growth of the biomineral is a carefully controlled, cell-mediated process. However, precipitation can also be 'biologically induced' or 'biologically influenced' (Figure 26). Here, microorganisms are most often involved. While both types of precipitation typically occur outside of cells, a distinction between the two processes is important. 'Biologically induced' precipitation is a direct result of microbial activities, which generate the biochemical conditions necessary to facilitate precipitation. 'Biologically influenced' precipitation is a passive process, and a result of interactions between extracellular biopolymers and the geochemical environment [37].

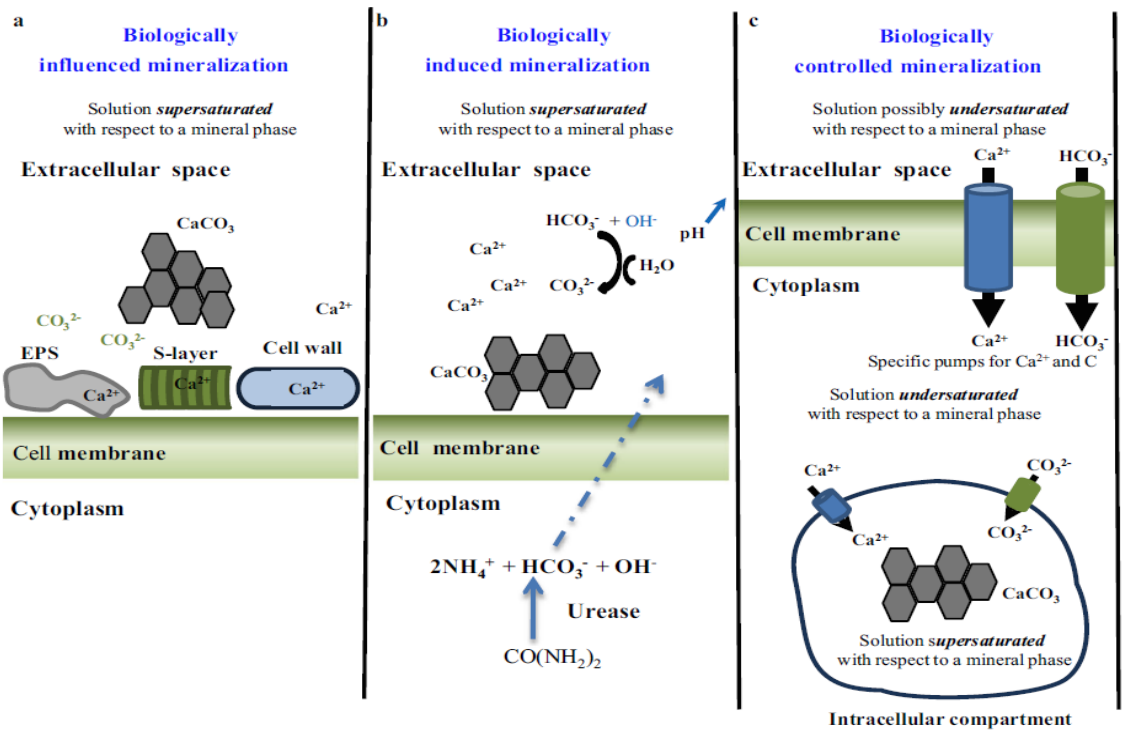

Figure 26: Classification of the $CaCO_3$ biomineralization processes found in bacteria: a biologically influenced mineralization; b biologically induced mineralization; c biologically controlled mineralization [19].

Microbially induced calcium carbonate precipitation (MICP) has been studied extensively in recent years and has implications in many environmental applications, including but not limited to aquifer decontamination, soil stabilization, and carbon capture and storage (CCS). The hydrolysis of urea (NH_2CONH_2) (i.e., ureolysis) by native or introduced microorganisms is one of several microbial pathways that can be used to induce *in-situ* $CaCO_3$ precipitation [38]. Ureolysis produces ammonia (NH_3) and dissolved inorganic carbon (DIC), which increases alkalinity, ultimately favoring the precipitation of $CaCO_3$ in the presence of dissolved calcium. The precipitation of $CaCO_3$ is governed by the following parameters: calcium concentration, DIC, T, pH, and the presence of nucleation sites. Bacterial cells have been shown to function as nucleation sites, and studies have confirmed the precipitation of $CaCO_3$ on bacterial cell surfaces

3.2 STRUCTURE OF BIOFILMS AND ACTION OF EXTRACELLULAR POLYMERIC SUBSTANCES – BIOLOGICALLY INFLUENCED MINERALISATION

A biofilm is a complex microbial consortium of surface-dwelling microorganisms that are enmeshed in a polymeric matrix of polysaccharides and other macromolecules called the extracellular polymeric substance (EPS). EPS are a complex mixture of high-molecular-weight polymers, mostly composed of polysaccharides with some nucleic acids, lipids, proteins, and other polymers such as humic acids [39]. EPS are a major component of biofilms, sometimes accounting for more than 90% of their dry mass, and support the aggregation of cells and attachment to surfaces [40].

Such EPS, can be separated into two fractions: an EPS gel and soluble EPS. Both fractions are rich in xylose, fucose and glucuronic acid. The EPS gels contained large amounts of 3-linked, 4-linked and 3,4-linked fucose, 3,4-linked glucuronic acid and terminal xylose linkages. The EPS gel consisted of a fibrillar

matrix that linked cells and cell substrate together [41]. This is just one example that shows one of the principal components in EPS. Regardless, a wide range of organic molecules is found associated with the EPS matrix; some of which are structural components, while others are adsorbed or localized molecules. The distinction between the two, however, is not often clear.

There are still diverging views about how EPS are involved in carbonate precipitation. In some cases, it has been proposed that acidic polysaccharides inhibit carbonate precipitation [42]. As a result, carbonatogenesis may occur in EPS-poor areas only, where high concentrations of Ca^{2+} and Mg^{2+} have been released by the degradation of polysaccharides by heterotrophic bacteria [43]. Alternatively, it has been speculated that EPS may transform upon decay into a highly organized template structure favoring calcium carbonate nucleation and as such enhancing precipitation of calcium carbonate [44]. Functional groups on EPS serve as initial nucleation sites, while other moieties function to control extent and types (e.g., crystals vs. amorphous organo-minerals) of precipitation. Giuffre et al. [45] showed that charge density is a prominent parameter to predict the impact of EPS on nucleation - the higher the charge density (e.g., presence of highly sulfated or carboxylated polysaccharides), the greater the energy barrier for nucleation. As a result, EPS with higher charge density induce higher nucleation rates at higher supersaturation indices of the solution, while at lower supersaturation indices, near-neutral EPS macromolecules induce higher nucleation rates. Structural variations in EPS impact nucleation rates to a lower extent than charge densities. Moreover, the EPS composition with respect to uronic acid, carbohydrates and protein influence carbonate polymorphism in vitro [42], with some EPS favoring aragonite precipitation, while others favor calcite formation. Furthermore, Han et al. recently showed that EPS produced by *Bacillus subtilis* [46] contain abundant acidic amino-acids such as glutamic acid and aspartic acid, and act as nucleation sites for carbonate mineral phases in supersaturated solutions.

Despite the considerable amount of literature available on biomineralization in general, biomineralization in geothermal or similar environments has been the subject of few studies (e.g., [47]). Given the extreme nature of geothermal systems and the lack of knowledge regarding their biocenosis, we argue that particular care must be taken when applying existing knowledge on biomineralization to organisms that inhabit these brines. In this study we aim to use available literature on biomineralization and geothermal organisms to construct a framework understanding of the main ways in which organisms could impact mineral scaling in geothermal infrastructures. We also aim at determining which key research topics would need to be developed to be able to better characterize the impact of microorganisms in the geothermal environment.

We complement this approach with two observational experiments to investigate one particularly controversial pathway of biomineralization: biomineralization influenced by microbial surface properties. Already proposed by Thompson and Ferris [48], the potential role of microbial surfaces in the nucleation of crystals has been explored more in detail by Douglas and Beveridge [49], who claim that highly specific surfaces and charged surface functional groups make bacterial cells capable of interacting with ions in solution, therefore making them ideal centres for crystal nucleation. The charged surface functional groups allow the organism to interact with cations in solution and adsorb them, therefore the cations become more concentrated in the immediate surrounding of the cell. Consequently, the cell becomes a hotspot for cation-anion interaction, causing preferential precipitation of minerals at the cell's surface. This claim however has been challenged. For example, Ansari et al. [50] who found no effect of microbial surfaces on calcium carbonate precipitation and proposed instead that nucleation properties of bacterial cells may be tied to the activity of their calcium channels. This would make nucleation dependent on the microorganism's activity and therefore arguably not due to the inherent physico-chemical properties of its surface. Moreover, even

articles supporting the claim from Douglas and Beveridge [49] have declared that cation adsorption may in fact not be responsible for the observed behaviour. Perito et al. [51] visually assessed that inactive *B. subtilis* cells can increase the amount of calcium carbonate precipitation in a solution and attributed this increase to the nucleation capabilities of the surface of the cells. To verify if cations adsorption was responsible for the observed behaviour they chemically stripped the cells of adsorbed cations and found that their effect on the precipitation of the minerals was not reduced. They therefore concluded that cation adsorption was not relevant to the phenomenon. However, in our opinion, because they stripped the adsorbed cations before placing the cells in the precipitation solution, this does not guarantee that the cells did not adsorb additional cations afterwards, and that this allowed the cells to nucleate the minerals.

The microbial surface nucleation model is essentially based on the observation of environmental samples in which minerals are often found in close spatial association with bacterial cells. This nevertheless does not establish a clear causal relationship between microbial presence and changes to mineral precipitates, rather it suggests the possibility of an interaction between the two. The spatial relationship between cells and minerals is often investigated by electron microscopy (e.g., Thompson and Ferris [48]), which offers very detailed imagery of the interaction between crystals and cells but requires the samples to be dried. The process of drying the samples will certainly cause ions in the remaining fluids to crystalize. Therefore, it may significantly alter the position, morphology and quantity of crystals compared to what would be observable while the biomass was still wet or submerged in a fluid. For these reasons we find that, while sufficient evidence for an interaction between inactive microbial cells and minerals is present, direct evidence in favour of nucleation of minerals on microbial cell surfaces is scarce. Therefore, using two experimental approaches, we aim at investigating the fundamental question of whether or not microbial cells can act as nucleation sites for the formation of crystals when precipitation occurs in a solution. Our hypothesis is that bacterial and fungal cells will act as nucleation sites for the formation of crystals.

3.3 BIOMINERALIZATION INFLUENCED BY MICROBIAL SURFACE PROPERTIES

Two experiments were conducted in a calcium carbonate precipitation solution that is not intended to simulate a geothermal brine, but rather to provide a supersaturated liquid environment where mineral precipitation can occur in the presence of submerged cells. The solution has a simple chemistry (see below) and selectively precipitates calcium carbonate. This mineral was selected because it has been extensively studied in the context of biomineralization (e.g., Seifan and Berenjian [52], Görgen et al. [37]), allowing for a more direct comparison with results from the existing literature. The precipitation solution did not contain any energy source for the organisms, which is done intentionally to prevent any contribution of microbial metabolism to mineral precipitation acting as a confounding factor. The distinction between biomineralization due to surface properties or to metabolic activity was essential in our experiments and was explored in detail by Ansari et al. [50].

In the first experiment, the precipitation of calcium carbonate was induced in the presence of different microbial cells. This method was termed static observational approach, as the samples were analysed by optical microscopy only after the precipitation has taken place. The aim of the experiment was to observe the spatial relationship between crystal and cells, mainly to determine whether cells with crystals attached to their surfaces or crystals with cells attached to their surfaces were present. This experiment also allowed to monitor if and how the morphology of the crystals is affected by the presence of the biomass. If microbial cells with crystal overgrowth were to be found, the hypothesis that cells can act as nucleation sites will be supported. For this experiment *Bacillus subtilis* was chosen as a model bacterium as its inactive cells have already been shown to be able to impact calcium carbonate precipitation) [51]. No such strong candidates were found in existing literature for fungi,

therefore *Penicilium commune* was chosen as a readily available, easily culturable, model fungus. A newly isolated geothermal bacterium, *Thermaerobacter* sp. was also used as a representative of the extremophiles that can be found in geothermal brines, providing a link to the wider scope of this work.

The second experiment expands on the aims of the static observational experiment. Thanks to the use of a fluorescently tagged bacterium (*Pseudomonas putida*), it was possible to improve the detection of cells during observation. Cells could also be observed through crystals, allowing to identify potential biological inclusion in larger crystals. An inverted microscope was used to let the fluid rest undisturbed during observation, and the precipitation solutions were mixed directly on the glass slide and quickly put under the microscope. As this allowed to observe the dynamic of the mineral precipitation in the solution this experiment is referred to as the dynamic observational approach. If nucleation at the cell surface occurs, this method should allow us to directly witness the formation of the crystal and its growth. If crystals will be observed growing on the surface of the bacterial cells, the hypothesis that microbial surfaces can act as nucleation sites for minerals will be supported.

3.3.1 Microbial strains and culture conditions

All the strains originated from the collection of the Laboratory of Microbiology at the University of Neuchâtel. *B. subtilis* and *P. putida* were cultured at ambient temperature in the dark on Nutrient Agar (NA) plates. The NA medium was prepared by mixing 15 g of Agar technical powder (Biolife) with 25 g of Standard Nutrient Broth I powder (Roth) in 1 L of deionized water before autoclaving. *Thermaerobacter* sp. was cultured at 60°C in the dark on Marine Agar (MA) plates. The MA medium was prepared by mixing 15 g of Agar technical powder (Biolife) with 37.4 g of Difco Marine Broth 2216 powder (BD) in 1 L of deionized water before autoclaving. The fungus *P. commune* was cultured in 50 ml flasks of Malt Broth at room temperature in the dark under constant agitation at 110 rmp. The Malt Broth medium was prepared by dissolving 12 g of Malt Extract powder (SIOS Homebrewing) in 1 L of deionized water before autoclaving.

3.3.2 Precipitation solutions

Two stock solutions for mineral precipitation were prepared by dissolving $NaHCO_3$ (Sodium bicarbonate powder, Sigma-Aldrich) in deionized water at a concentration of 0.25 M and $CaCl_2$ (Calcium chloride dihydrate, Roth) in deionized water also at a concentration of 0.25 M. The solutions were then sterilized by filtering them through a syringe fitted with a Millipore 0.22 µm polyethersulfone filter attachment (Merck Millipore) into sterile glass bottles and stored at ambient temperature in the dark. These solutions provided the necessary ions for the precipitation of calcium carbonate in both the static and dynamic experimental approaches. Sterile deionized water (SDW) was also prepared by filtering regular deionized water through a syringe with a Millipore 0.22 µm filter attachment (Merck Millipore) into a sterile glass bottle and was also stored at room temperature in the dark.

3.3.3 Static observational approach

The biomass was collected using a plastic loop from an overnight culture of *B. subtilis* and a 48h culture of *Thermaerobacter* sp. and suspended in 1 ml physiological water. The biomass was then washed by centrifuging at 3000xg for 10 minutes, removing the supernatant and resuspending it in 1 ml physiological water. To collect the fungal biomass, a 50 ml overnight liquid culture of *P. commune* was pelleted by centrifuging at 4000xg for 15 minutes, the supernatant was removed, and the pellet was resuspended in physiological water. To wash residual media, the fungal biomass was pelleted again by centrifugation as before, the supernatant was removed, and the pellet was finally resuspended in 1 ml

physiological water. Both precipitation solutions, the one containing $CaCl_2$ and the one containing $NaHCO_3$, were diluted to a concentration of 41 mM for this experiment. Higher concentrations were used in preliminary tests, but they produced an excess of precipitates that would occlude observation of the cells. On the contrary lower concentrations instead produced either extremely small or very few crystals per sample. A concentration at 41 mM therefore offers a suitable number of crystals to be observed throughout the sample without impeding the view of the cells. For each organism, 1 µl of the biomass suspension was added to 500 µl of the diluted $CaCl_2$ solution in separate 1.5 ml Eppendorf tubes. The amount of suspension to be added to the precipitation solution was chosen as it provides a final concentration of cells that is high enough to be easily found among the crystals, but not high enough to make the cells indistinguishable from one another. This is key in order to detect the growth of crystals on the surface of each singular cell. The solution was left to rest for 30 minutes to allow the cells to interact with the ions in solution. Then 500 µl of the diluted $NaCO_3$ solution were added to cause $CaCO_3$ precipitation. The solution was mixed and finally 20 µl of the solution containing the biomass and precipitates was transferred to a glass slide, covered with a coverslip, and observed under an optical microscope (Leica DM4 B) fitted with a Leica DFC7000 T camera. Phase contrast was used to enhance the visibility of bacterial cells. Samples of the two solutions containing only the ions and samples of physiological water containing only the bacterial or fungal cells were also observed as negative controls for the morphology of the crystals and the aspect of the microbial cells respectively. The controls and the samples containing each organism were prepared in triplicates for a total of 21 samples. The samples were observed three times each for a total of 63 observations.

All twenty-one samples showed nearly identical calcium carbonate morphology. The precipitates always consisted of highly angular rhombohedral crystals, of size comprised between 10 µm and 1-2 µm. Some different morphologies have also been observed, which include but are not limited to large (>50 µm) fan shaped crystals, large angular or cubic crystals and more rounded medium (20-40 µm) sized crystals. These morphologies do not appear to be linked to any of the treatments and appeared both in the presence and in absence of biomass. Their abundance is extremely low, as only one to five crystals per sample were observed. In general, it can be said that the presence of fungal and bacterial cells in solution did not affect the morphology of the calcium carbonate. As can be seen in Figure 27 none of the organisms tested displayed any affinity to the precipitates. No crystal was seen adhering to the surface of any cell throughout all samples. The surface of the cells was always smooth and uninterrupted as in control samples containing only cells without addition of ions. The surface of the observed crystals was also free of any cells. The fact that precipitates were found deposited at the bottom of the solution, in contact with the glass slide, while the organisms tended to float in the solution, further marks the spatial separation of the mineral and biological phases. Due to the floating behaviour of cells, some cells are superposed to the precipitates. The superposition is clearly visible in Figure 27C. but also visible is the fact that the crystals are entirely out of focus, therefore the precipitates are relatively distant from the cell. Due to their metabolisms, both samples containing *B. subtilis* and those containing *P. commune* also contained some spores of these organisms. These spores when present behaved identically to the vegetative cells in regard to the mineral precipitates, showing no crystal overgrowth or affinity to the crystals. Additional pictures of this experiment are available in the supplementary materials.

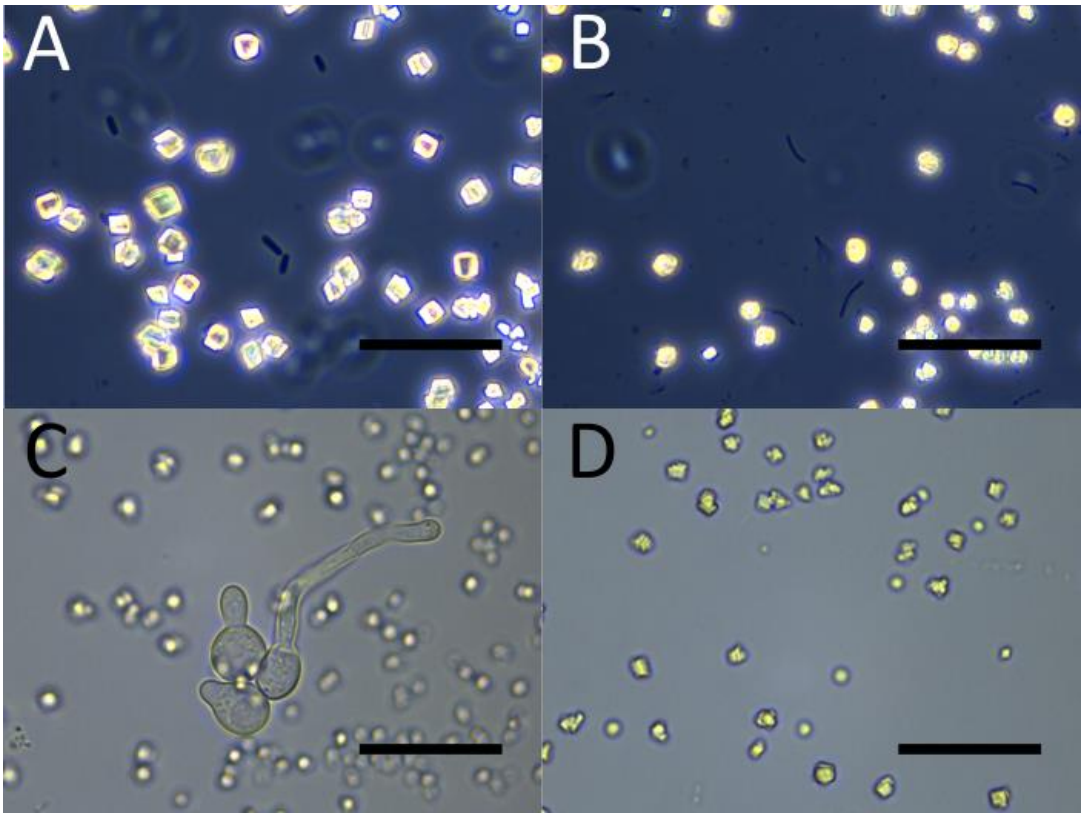

Figure 27: Selected results from the static experimental procedure. A) *Bacillus subtilis* cells showing no crystal overgrowth. B) *Thermaerobacter* sp. cells showing no crystal overgrowth. C) *Penicillium commune* showing no crystal overgrowth, note how here the crystals are significatively out of focus indicating that the fungus is floating above the precipitates. D) Solution without biological cells the precipitates have similar morphology and size to the ones in images A, B and C. Scalebars are 20 micrometres. Images obtained by Isacco Darini (UNINE).

The static experimental approach found no clear evidence of mineral nucleation on microbial surfaces. Its results therefore do not support the initial hypothesis that microbial cells can act as nucleation sites for mineral formation. This first experiment acted as a simple preliminary test, that could have detected only clear signs of crystal growth on microbial surfaces in a qualitative manner. It must be said that, given the observational nature of this experiment, nucleation of crystals at the cell's surface could have occurred and not be detected. The first possibility for this is that crystals could have initially nucleated on cells but may have detached as they grew larger or due to the mechanical agitation as the solution was mixed and transferred via micropipette to the glass slide. Secondly it is possible that some crystals may have entirely engulfed the cells after nucleation. However, the latter would only have been possible for bacterial cells, as crystals large enough to contain fungal cells were not observed in any of the samples. These issues underline the need for an improved experimental design where crystallization can be observed without the need for a transfer that induces mechanical disturbances. An ideal approach would be one that allows to monitor the precipitation as it is occurring. The dynamic experimental approach was developed precisely with this intent.

3.3.4 Dynamic observational approach

The biomass from an overnight culture of *P. putida* was collected using a plastic loop and suspended in 5 ml physiological water. To prepare the precipitation solutions, 500 µl of $NaHCO_3$ and $CaCl_2$ solutions were placed in different 1.5ml Eppendorf tubes and diluted using 500 µl of SDW for each to reach a final concentration of 125 mM. This concentration was chosen after preliminary tests using different concentrations, showing that it allows for the precipitation to take place at a slow enough

pace to be meaningfully observed, but fast enough to occur before the evaporation of the drop. The latter is particularly important in the scope of maintaining the organisms submerged in the solution as the precipitation occurs, mimicking the conditions of an actual fluid. Afterwards, 5 µl of cell suspension was added to 1 ml to the diluted $NaHCO_3$ and $CaCl_2$ solutions. Lastly 5 µl of each of these solutions, containing both ions and cells, were placed on a 24x60 mm coverslip, and mixed in a single drop. The cover slip was then transferred as fast as possible to an inverted microscope (Invitrogen EVOS M5000, Thermo Fischer scientific) and observed in green fluorescent light and transmitted light. To capture the evolution of the precipitation as it is occurring, time lapses were assembled by taking pictures at 10 seconds intervals for 3 to 5 minutes after the merging of the two solutions. Observation of the samples generally started at the earliest 45 seconds after the merging of the two solutions, and as evaporation becomes an important factor over time, it was not possible to observe the samples for longer than 10 minutes. The built in Z-stack function of the microscope allowed to obtain better images of larger crystals that span over several focus planes. Twenty-one samples of precipitation solution containing bacterial cells were prepared and observed. Samples of the precipitation solution without addition of biomass were used as negative controls for the morphology of the crystals, of these samples 7 replicates were prepared and observed. To verify that the aspect of the bacterial cells was not modified by the precipitation solution, bacterial cells suspended in physiological water were observed. For this, three samples were prepared by diluting 5 µl of bacterial suspension in 1 mL of physiological water to match the dilution of the other samples and observed.

With the method used in this experiment it was possible to observe the crystals as they are forming in solution. This allowed to clearly determine the nucleation point of the crystals. In all 21 samples containing bacterial biomass no crystal was observed nucleating on any bacterial cell. Contact between cells and crystals was observed only when crystals formed in suspension and came in contact later on with cells, or when the cells moving passively in the fluid came to rest against an already growing crystal. The use of bacteria constitutively expressing green fluorescent protein allows to observe cells trough crystals, therefore cells encased in large crystals could be detectable if present, however no cells where visible through any of the crystals that were observed. The seven control samples without the addition of biomass all behaved similarly. Figure 28 shows that within one minute from the mixing of the solutions a large number of very fine (< 1 µm) crystals appeared alongside larger (5-10 µm) rhombohedral ones. Then, during the observation window (5-7 minutes), the larger crystals grew, usually doubling in width by the third minute. The very fine crystals developed in a dense fine crystal matrix by having new minute crystals nucleate at their ends.

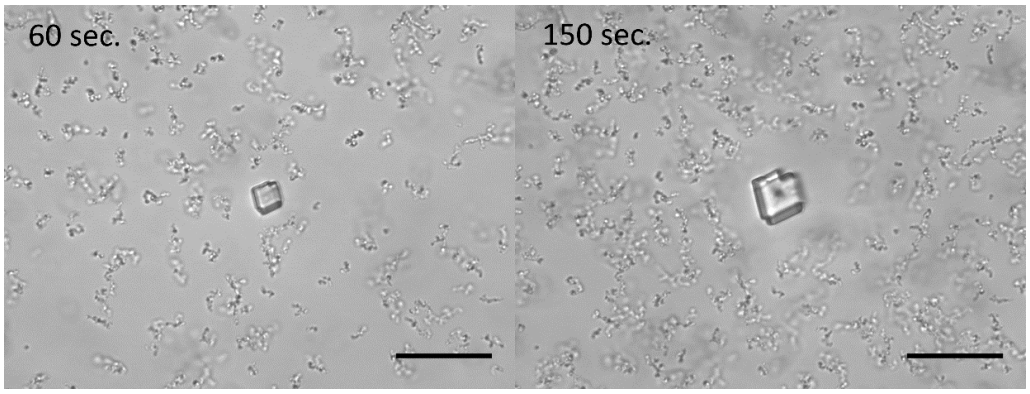

Figure 28: Results from the dynamic experimental procedure. Precipitation of calcium carbonate without addition of bacterial cells. Evolution of precipitation from ca. 60 seconds to ca. 150 seconds after merging of the two solutions. In the centre an angular crystal can be seen growing surrounded by an increasingly dense matrix of filamentous agglomeration of very small crystals. Scalebar is 20 micrometres long. Images obtained by Isacco Darini (UNINE)

In the samples where bacterial cells were present, differences in the evolution of the precipitation and morphology of the crystals were detected. Nine of the twenty-one samples developed identically to the control samples: with the simultaneous precipitation of both the dense filamentous matrix and the growth of larger angular crystals, as can be seen in Figure 29. While in the remaining twelve samples the formation of an early stage of filamentous matrix followed by the formation of larger (5-20µm) crystals with rounded shape and irregular edges, accompanied by the dissolution and disappearance of the filaments of small crystals, as can be seen in Figure 30.

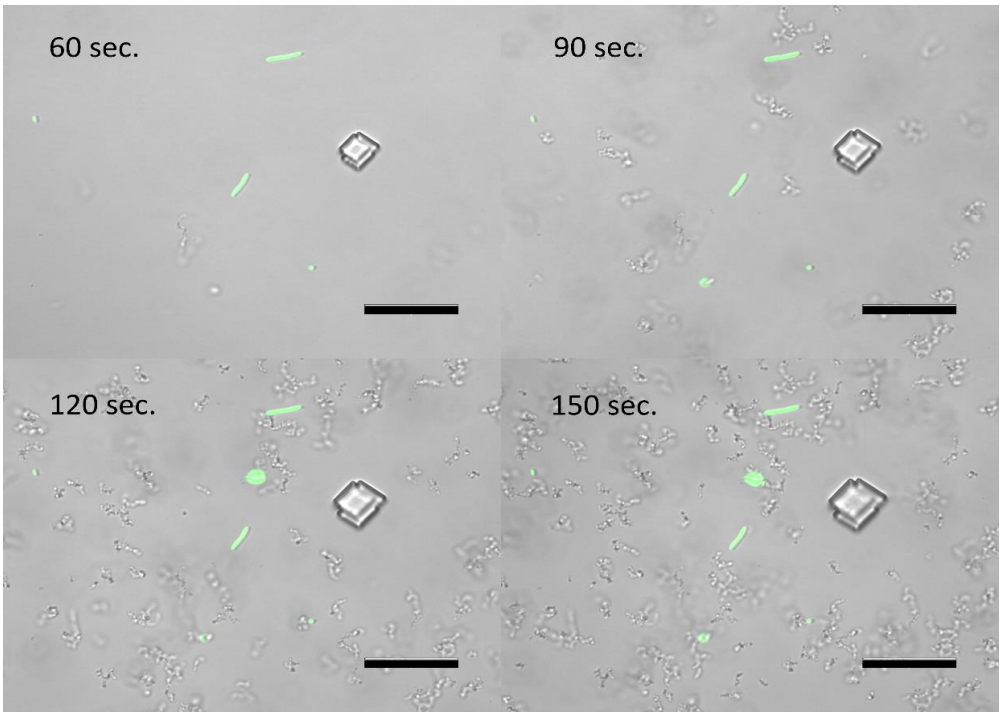

Figure 29: Results from the dynamic experimental procedure. Precipitation of carbonate in the presence of bacterial cells. Evolution of precipitates from 60 seconds to 150 seconds after merging of the solutions. Bacteria are highlighted in green thanks to the superposition of transmitted light and fluorescent light images. Scalebars are 20 micrometres. Images obtained by Isacco Darini (UNINE)

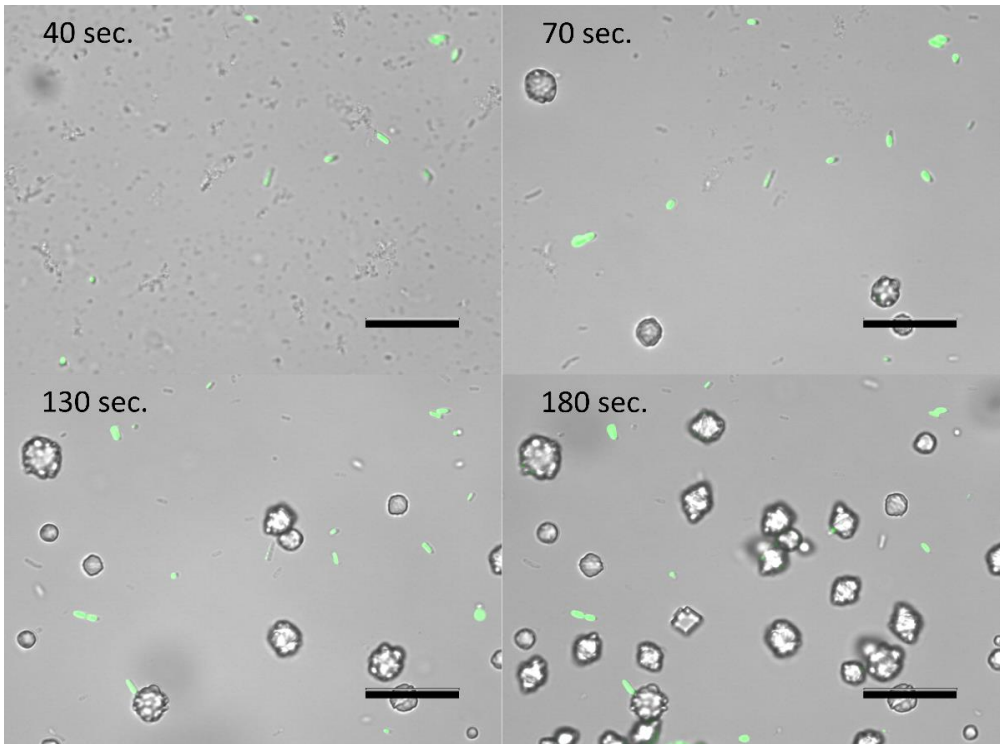

Figure 30: Results from the dynamic experimental procedure. Precipitation of calcium carbonate in the presence of bacterial cells. This sample shows different crystal morphologies, angular crystals are present along a majority of more rounded irregular ones. Evolution of the precipitation from 40 seconds to 180 seconds after merging of the solutions. On the top left image, the early stage of a filamentous matrix is visible, it then dissipates in favour of the larger rounded precipitates. Bacteria are highlighted in green thanks to the superposition of transmitted light and fluorescent light images. Scale bars are 20 micrometres long. Images obtained by Isacco Darini (UNINE).

The use of a drop under an inverted microscope allows for the solution to sit undisturbed. Mixing the solutions directly on the microscope slide eliminates the need to transfer the solution and therefore does not cause any additional disturbances. Moreover, the use of fluorescently tagged bacteria allows not only to detect bacteria through crystals, but also to quickly identify and focus on the cells at the start of the observation. These three factors combined allow for the observation of the undisturbed precipitation of minerals in the solution as it is occurring. As it can be seen in Figure 29 this method indeed allows to track the precipitation from its earliest stages, when crystals are still absent or mostly absent in the fluid. The nucleation of crystals on the surface of the cells was not observed in any sample. An abundance of crystals can be seen appearing and growing in all samples but never in contact with any bacteria. Furthermore, all crystals seem to be nucleating independently throughout the fluid. Therefore, our findings do not support the hypothesis that bacterial cells can act as nucleation sites for minerals.

Interestingly this approach revealed some differences in the precipitation dynamics and morphology of the crystals between control samples and some of those containing bacterial cells. While nine of the 21 samples containing bacteria showed an identical precipitation pattern to the control samples, rounded crystals with an irregular edge appeared in the remaining twelve samples. This modification is unlikely to result from the surface properties of the cells themselves for two reasons. Firstly, the crystals form independently from the cells, and they are never in contact with one another. Secondly, the effect is not generalized to all samples containing bacterial cells but only occurs in around half of the samples. Thus, this change must be due to a parameter that was not controlled in this experiment. Due to the observational and qualitative nature of this experiment it is impossible to determine which factor caused this variation in morphology, but some hypotheses can be made. A factor that could

explain this variation is the presence of EPS that could have been transferred along with the bacterial cells in the precipitation solution. In fact, Braissant et al. [53] found that the presence of EPS and ammino acids in a solution could lead to changes in the morphology of calcite and vaterite crystals precipitating in that fluid. In particular, they found an association between increased presence of EPS led to the formation of calcite crystals that were rounder compared to their rhombohedral abiotically precipitated counterparts. These rounded calcite morphologies are remarkably similar to the ones observed in our experiments (Figure 30). Further supporting this hypothesis is the fact that *Pseudomonas* spp. are often used as model organisms for biofilm formation and are known for abundant EPS production. The fact that not all samples containing bacterial cells showed this change in crystal morphology can be explained by, for example, differences in the EPS produced by bacteria or in the amount that was incidentally transferred at the start of the experiment.

Even though our experiments do not reproduce the *in-situ* conditions of a geothermal brine, they yield new insights into the process of influenced biomineralization at room temperature. This insight can be integrated with the existing literature to increase our understanding of biomineralization.

3.4 BIOFILM FORMATION ON STEEL

When considering extremophilic organisms, often bacteria and archaea are in the picture. However, it is also possible that fungi could tolerate a large range of temperatures and that they constitute a natural component of the microbial diversity in geothermal systems. Consequently, in co-operation with Isacco Darini (Msc student at the University of Neuchâtel), it was explored whether biofilms on steel could induce biomineralization, accelerating the rate of clogging of the steel coupons. For this, two microorganisms isolated from geothermal environments (a bacterium and a mesophilic fungus, explained in detail below) were used. Using these biofilms in explorative experiments within TNO (with SR 45, T= 25 °C) it became clear, that EPS could initiate biomineralization, no matter if the organism that created this EPS is alive or not. However, when repeating the experiment at higher temperatures (70 °C), with or without flow and with even higher SR (up 70), the biofilm seems to dissolve completely and no specific scale formation could be found.

3.4.1 The microorganisms

Danaé Bregnard (PhD student at the University of Neuchâtel) found one thermophilic bacterium (*Thermaerobacter* sp.) and one mesophilic fungus (*Penicillium citrinum*) in two geothermal power plants and is currently characterizing them. *P. citrinum* is a fungus growing on citrus. It tolerates a large temperature range, going from 10 °C to 40°C [54] with an optimum at 30°C [23, 55, 56]. It also tolerates a large pH range. *P. citrinum* was isolated from geothermal fluids of the injection site in Heemskerk and could be grown on substrates for biofilm formation (Figure 31).

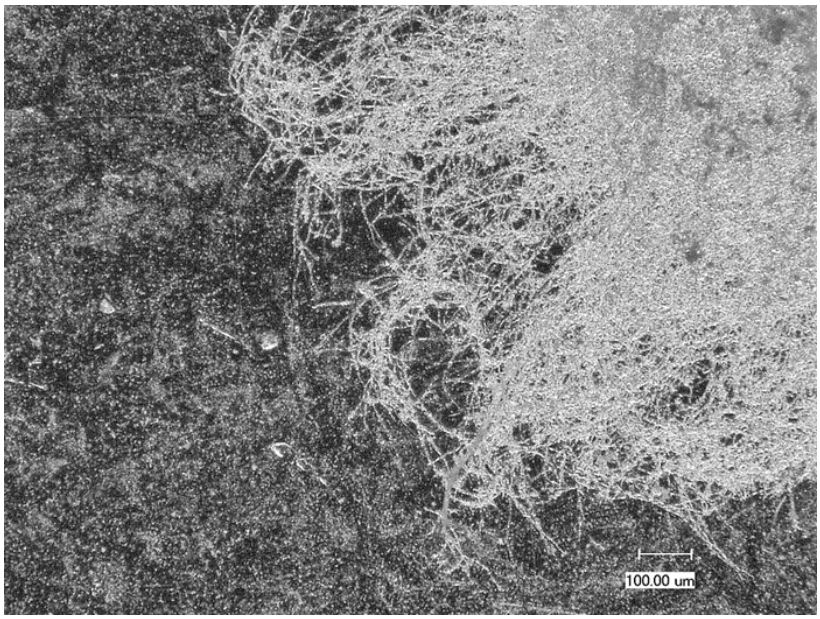

Figure 31: Optical micrograph of an example of *Penicillium citrinum* a s part of the biofilms on steel substrates as supplied by Kilian Blaise (UNINE).

The strain of *Thermaerobacter sp*. has not yet been assigned to a species for the moment. *Thermaerobacter* are Gram+ aerobic bacteria [33] and extremophilic thermophiles that tolerate a large spectrum of hot temperatures, going from 50°C to 80°C, with an optimum at 70-75°C [57, 58]. They also tolerate a wide range of pH, going from 5 to 10 [58], with an optimum at 7-7.5 [57]. *Thermaerobacter sp*. has been found in a geothermal station in Germany (Insheim). It was potentially in a dormant state in the geothermic water table.

3.4.2 Complex biofilm production

In continuation of the explorative experiments, these two organisms were grown on steel coupons by Kilian Blaise (student at the University of Neuchâtel). Five different configurations (based on growth media and order of inoculation) were tested for the creation of complex biofilms on rough and smooth steel plates. The biofilms grew in general better on smooth steel than on rough steel and that the inoculation of *P. citrinum* first on the steel plates in malt broth or Difco marine broth followed by a growth of *Thermaerobacter sp*. in Difco 2216 marine broth were the best combinations to obtain a complex biofilm (Figures 32 and 33). After drying, these coupons were transferred to TNO for the follow-up analysis (Figure 34).

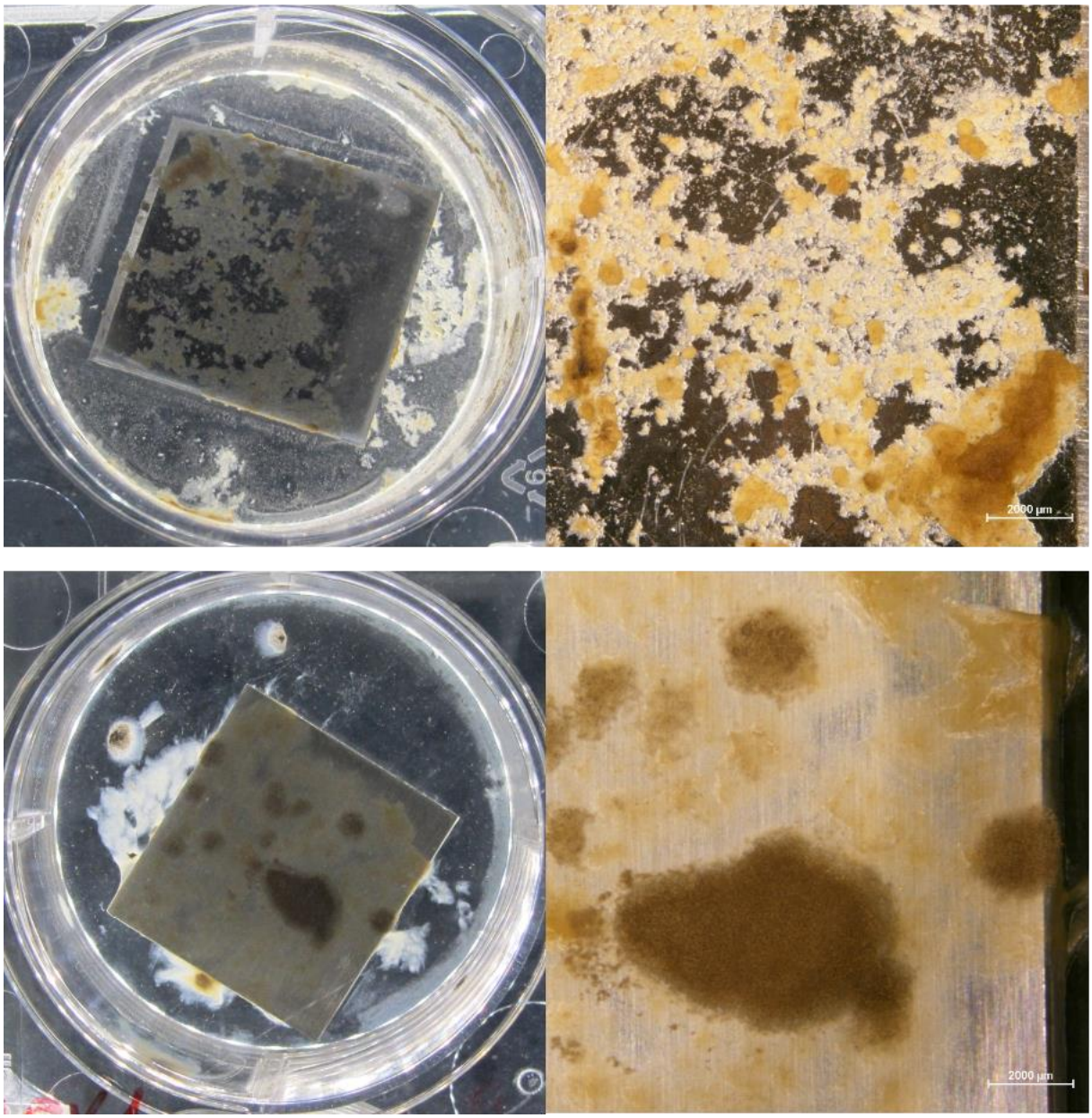

Figure 32: Growth of a complex biofilm on steel coupons (rough and smooth) where *P. citrinum* was grown in malt broth, and *Thermaerobacter* sp. In Difco 2216 marine broth. Top: Growth on smooth steel coupon and observation under the binocular. Bottom: Growth on rough steel and observation under the binocular.

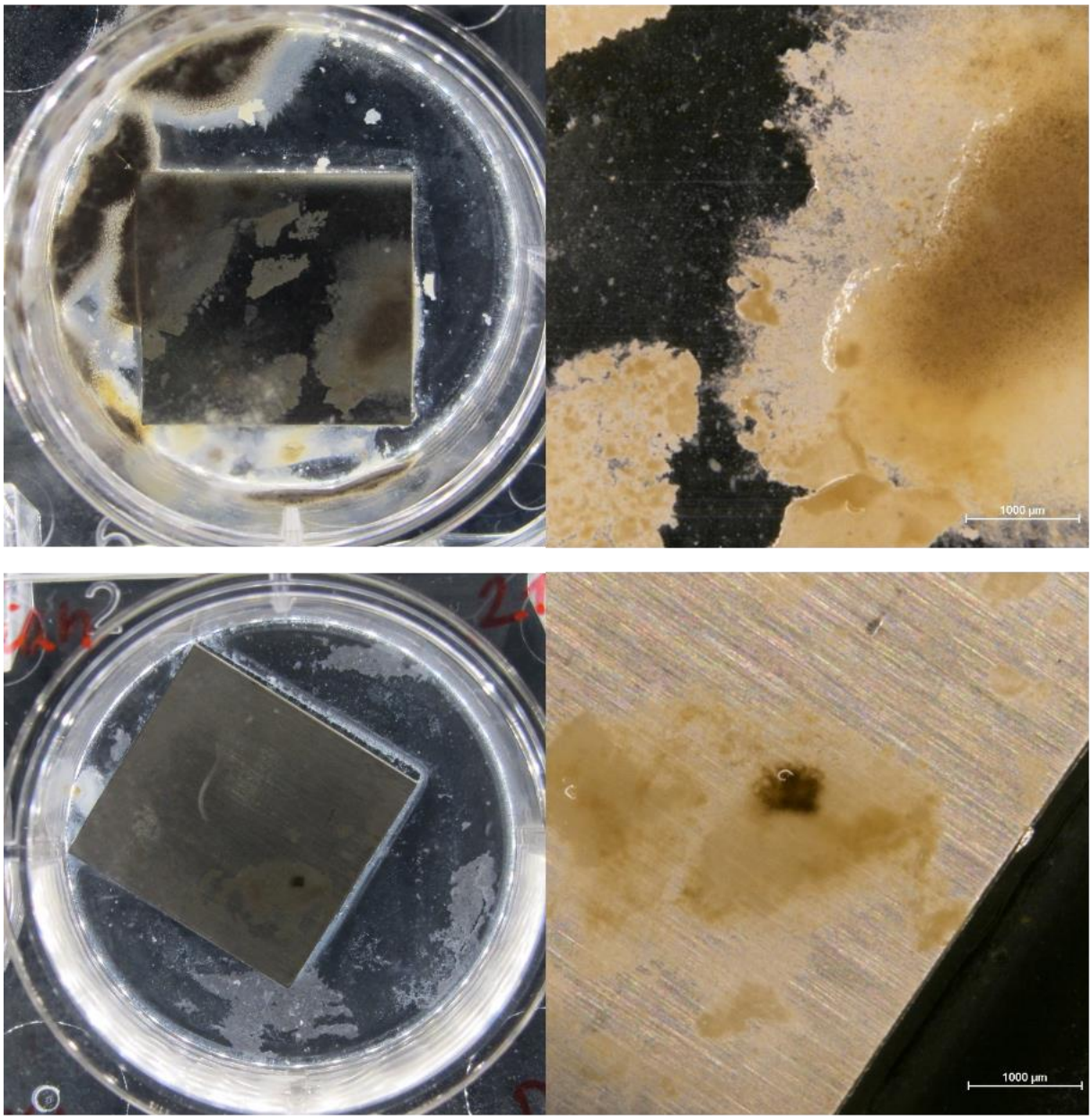

Figure 33: Growth of a complex biofilm on steel coupons (rough and smooth) where *P. citrinum* was grown in difco marine-malt broth and *Thermaerobacter* sp. in difco 2216 marine broth. Top: Growth on smooth steel coupon and observation under the binocular. Bottom: Growth on rough steel and observation under the binocular.

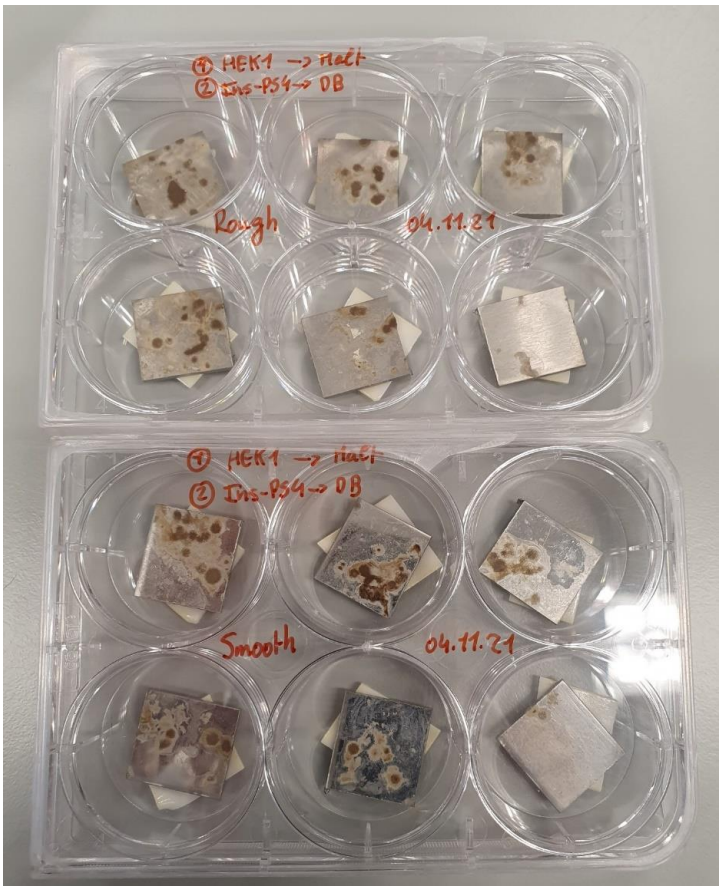

Figure 34: Examples of the biofilms on steel coupons biofilm as supplied by Kilian Blaise (UNINE).

Additionally, also a complex biofilm on an 80 cm steel plate was created by combining the fungus and the bacterium to be transferred to TNO to be used to monitor biomineralization in different solutions to evaluate their impact on nucleation. The growth of biofilms on the substrates (Figure 35) to be inserted in the large flow-loop set-up was somewhat more difficult and caused on some of the substrates' extensive corrosion. These extensively corroded samples were not useful for further experimental studies (Figure 36a). Other samples showed only minor corrosion and were used in a number of experiments as described in detail below (Figure 36b).

Figure 35: Images showing the setup use for the production of complex biofilms on 80cm steel plates. Ongoing incubation of *P. citrinum* in MA-filled Petri dishes on 80cm steel plates placed in the incubator at 30°C.

Figure 36: Examples of the biofilms on steel substrates to be used in the large flow-loop set-up as supplied by Kilian Blaise (UNINE). Extensive corrosion occurred (a, top images) as shown in the top images. Example of the biofilms on steel substrates used in the large flow-loop set-up as supplied by Kilian Blaise (UNINE; b, bottom images).

3.4.3 Experimental set-ups

Control over scaling parameters is important to fully understand the scaling process. To investigate the kinetics of scaling and the impact of biofilms present on scaling kinetics, two different types of set-ups were employed. Firstly, a scaling rig (Figure 37) with a flow loop was designed, allowing various combinations of scaling parameters as feed, temperature, supersaturation, residence time, etc., which are systematically investigated. The flow loop consists of an aluminum casing with a polyesteretherketone (PEEK) liner with connections for cooling water (Figure 38). The bottom is made of glass, separated by an O-ring. On top of the PEEK liner, a substrate with a length of 320mm and a width of 40mm can be inserted. On top of the substrate a PEEK casing with an O-ring is placed and the glass with the in- and outlet will be placed on top. The glass top is locked in place by placing the aluminum top and screwing it down until the O-ring fully seals the glass top. The brine solutions are prepared by dissolving $CaCl_2 \bullet 2H_2O$ and $NaHCO_3$ separately in 3 or 5L of water. The brines are pumped with Ismatec pumps (MCP-Z and BVP-Z) at 10 mL/min or 20 mL/min where they combine 10 cm before entering to the flow loop. Temperature and pH were controlled during the duration of all experiments.

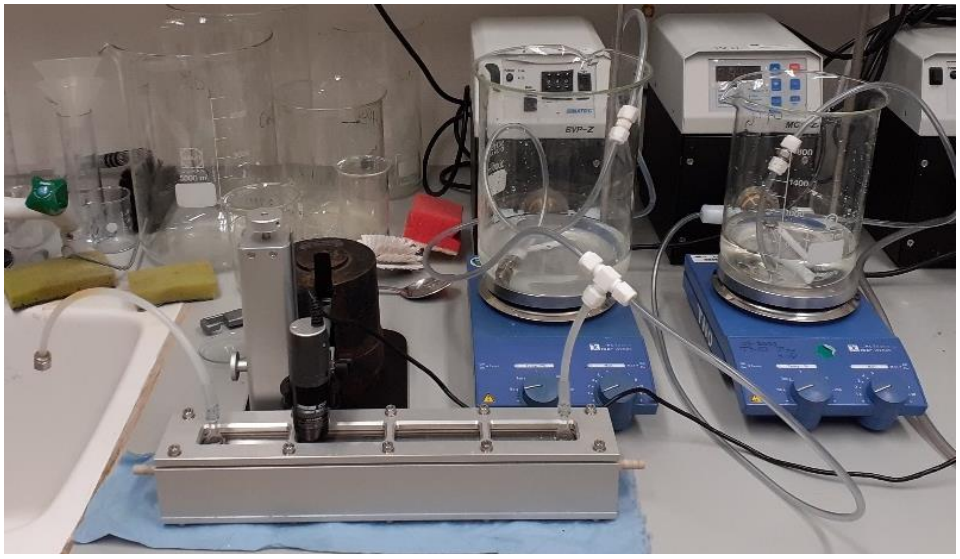

Figure 37: Small flow-loop scale deposition rig in operation.

The crystal growth is monitored in real-time using a Dino-lite camera placed on top of the glass focused on the surface of the substrate. The camera takes a picture of the substrate every 5 minutes. It is essential that the light intensity, focus, contrast and brightness are installed properly. To be able to run experiments also at higher pressure and temperature (up to 17 bar, 150 °C) a larger (10 cm by 81 cm) set-up was constructed with five built-in heating elements.

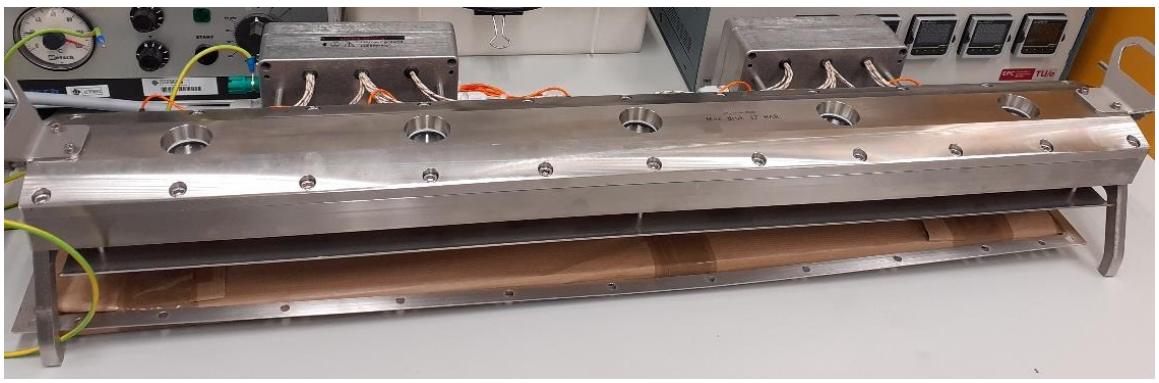

Figure 38: Large flow-loop scale deposition rig allowing studies under pressure and at higher temperatures.

Here, the set-up was constructed to enable first a flush with water containing one component ($CaCl_2$) to remove any air-bubbles in the system, to allow volume expansion during heating and the application of pressure. Via a by-pass construction the experiment was started by adding the second solution to the system when an equilibrium (temperature, flow, pressure) was achieved. With this set-up it was possible to generate data for deposition studies under pressure and elevated temperatures as input in the simulations of WP 4 (see Figure 39).

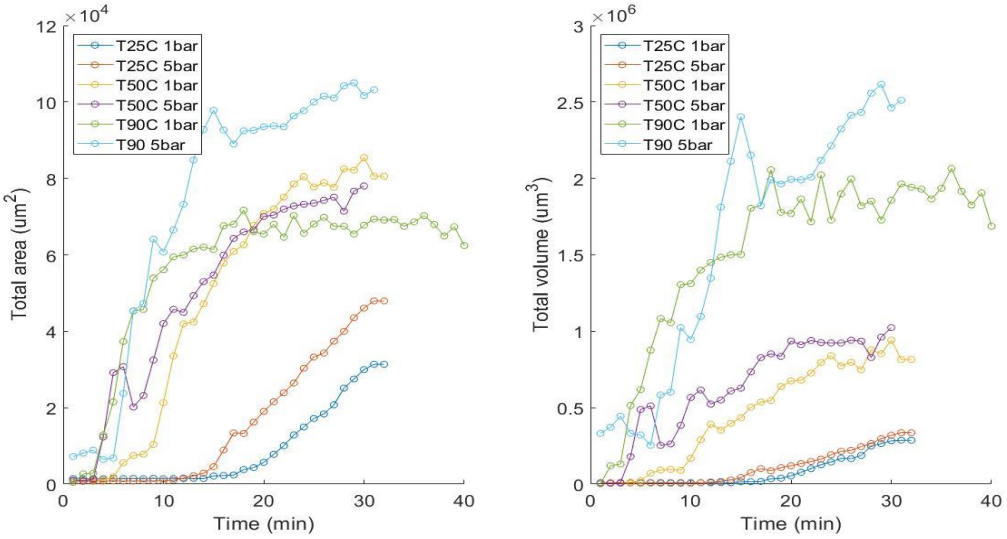

Figure 39: Scale deposition at variable pressure and temperatures.

Here it became clear, that pressure increase has only a very small (accelerating) influence on scale formation, therefore, the experiments on biofilm decorated samples were run at ambient pressure only. For a quick test of the influence of biofilms on scale deposition, a small-scale dynamic test set-up was assembled. The purpose was to screen the effect of biofilms grown on steel substrates on scaling formation at different temperatures. The solutions were added to the vessel shown in figure 40 and stirred slowly to mimic a small velocity flow.

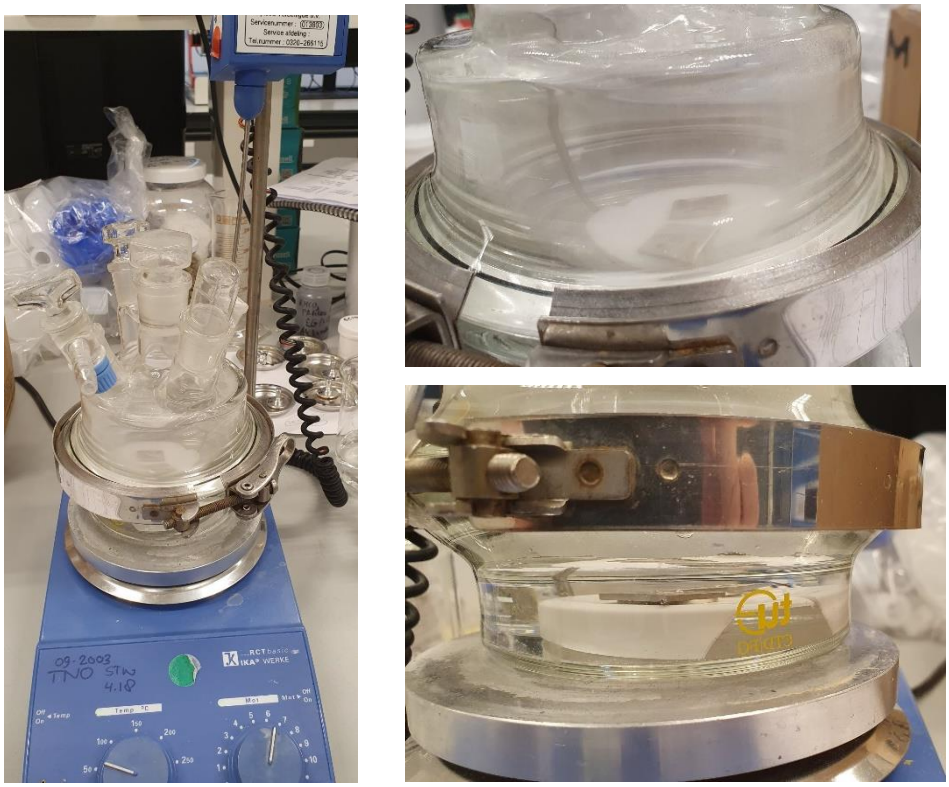

Figure 40: Small scale dynamic scale deposition set-up for screening of biofilm samples at higher temperatures.

Samples with biofilm and plain substrates as reference samples were tested and retrieved after 1 hour reaction time for analysis (microscopical inspection). The reaction temperatures of the experiments were 25, 50 and 70 °C. The reference samples showed a deposition/growth of calcite and vaterite on the steel substrate as described above (see Figure 41).

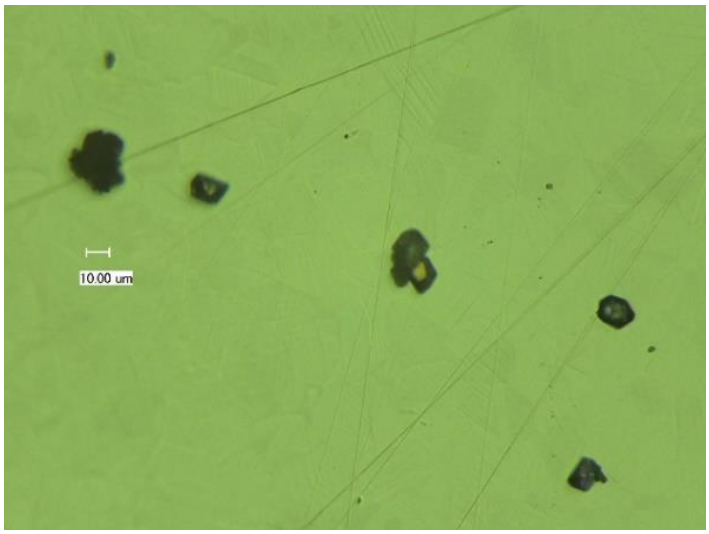

Figure 41a: Optical micrograph of the $CaCO_3$ precipitates/scaling formed at 25 °C after 1 hour reaction time on stainless steel substrates.

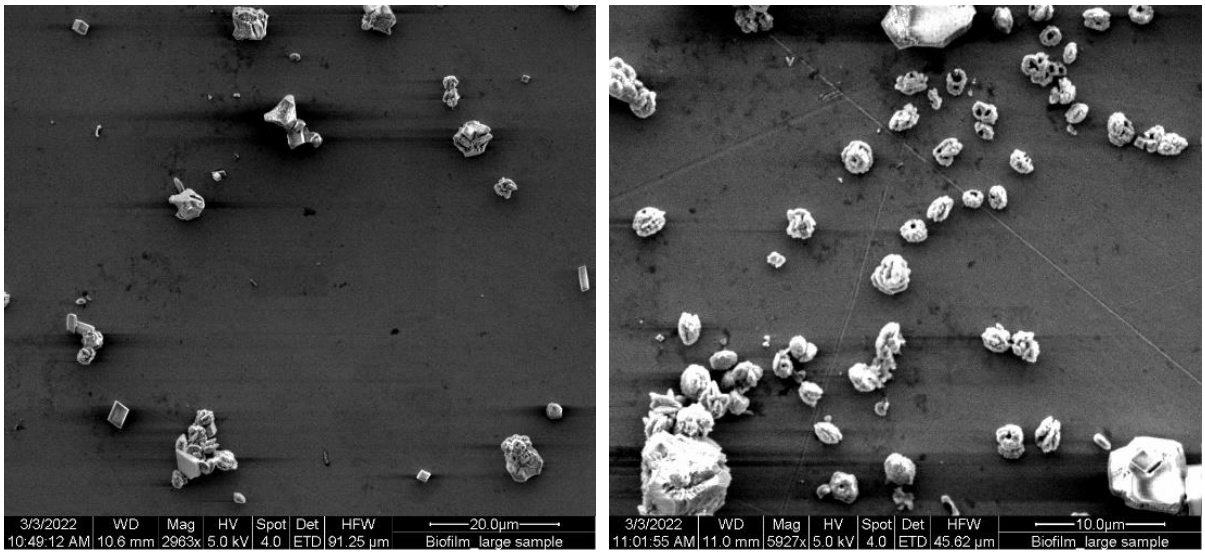

Figure 41b: SEM pictures of the $CaCO_3$ precipitates/scaling formed at 50 °C after 1 hour reaction time on stainless steel substrates.

The presence of the (mixed) biofilm clearly also shows scaling and precipitation, attached to the biofilm (Figure 42).

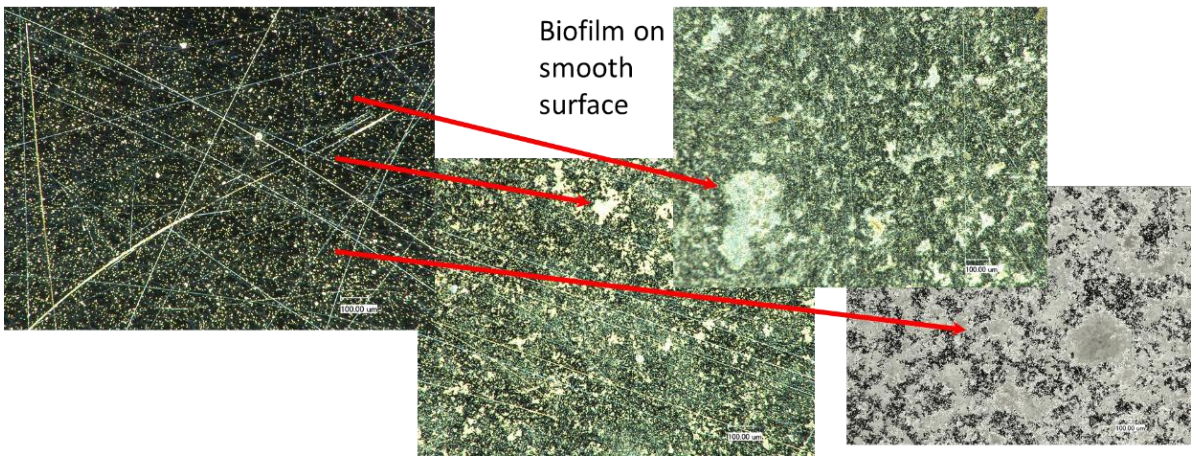

Figure 42: Optical micrographs of the $CaCO_3$ precipitates/scaling formed at 25 °C after 1 hour reaction time on biofilm containing stainless steel substrates, the reference sample (steel substrate) is the left picture.

It seems that the biofilm acts as a substrate for either precipitation or attachment of $CaCO_3$ crystals formed in suspension. Especially the *P. citrinum* covered areas seem to attach $CaCO_3$ (Figure 43).

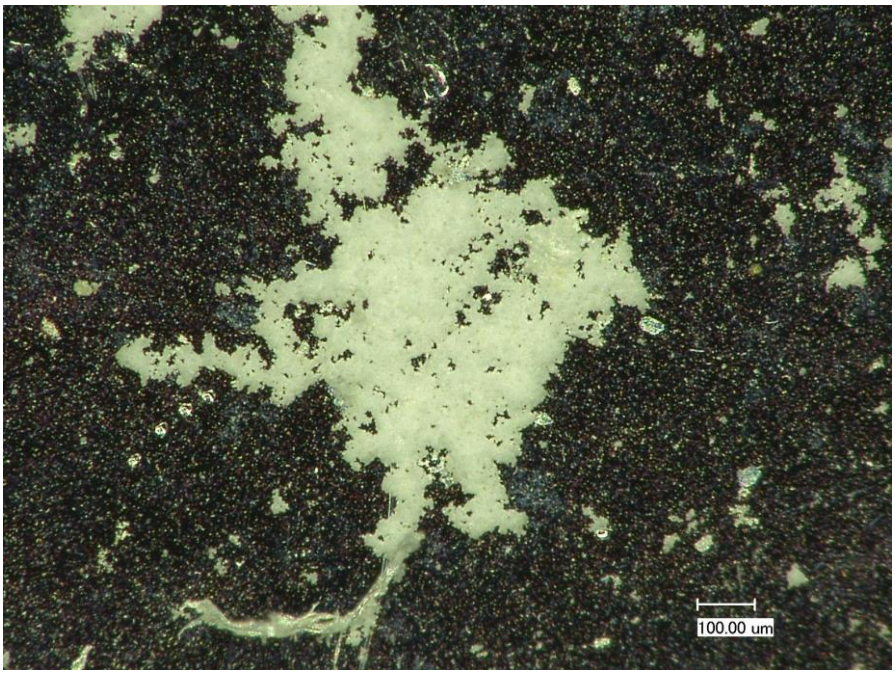

Figure 43: Optical micrograph of the $CaCO_3$ precipitates/scaling formed at 25 °C after 1 hour reaction time on attached to the *Penicillium citrinum* covered areas of the biofilm on stainless steel substrates.

Further details of the structures formed were explored using the SEM. The mycelium of *P. citrinum* seems to consist of highly branched networks of hyphae (filamentous structures). In low magnification pictures it seems that the whole filaments are covered with $CaCO_3$ particles, however, higher magnification reveals the existence of only very tiny, firmly attached $CaCO_3$ crystals to the hyphae (see Figure 44). An identification of the polymorph(s) formed was not possible.

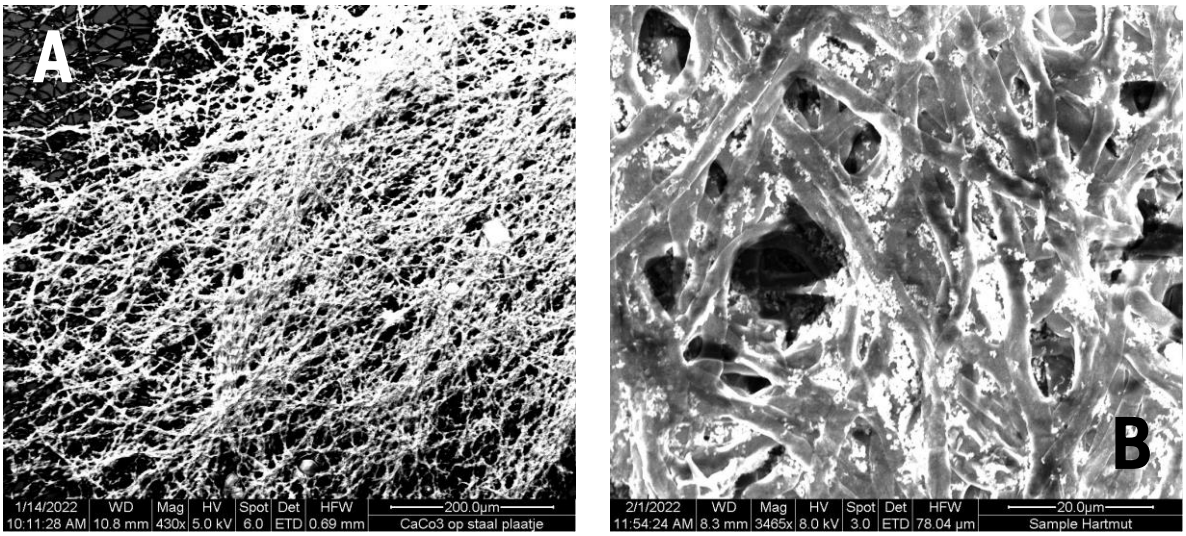

Figure 44: SEM pictures of the $CaCO_3$ precipitates/scaling formed at 25 °C after 1 hour reaction time on colonies of *Penicillium citrinum* covered areas of the biofilm on stainless steel substrates.

Other areas on the samples were clearly covered with an unspecific biofilm. Also, these areas were inspected after the experiment by SEM (Figure 45).

According to the appearance, mainly small vaterite crystals are formed again in close proximity to the biofilm. Only a few large calcite crystals, some possibly deposited from suspension after performing the experiment are observable (red circles).

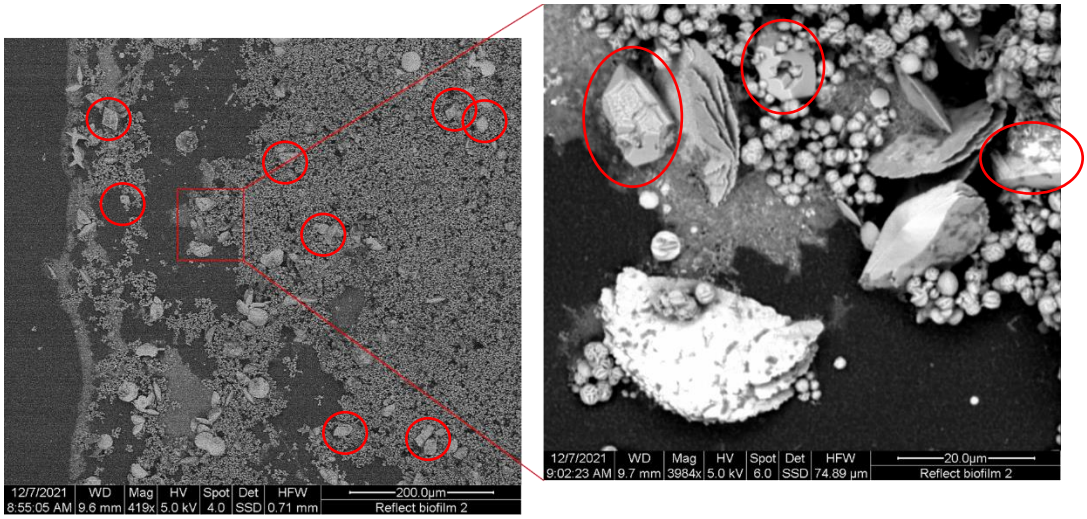

Figure 45: SEM pictures of the $CaCO_3$ precipitates/scaling formed at 25 °C after 1 hour reaction time on areas on stainless steel substrates covered with possibly EPS (gray film).

The picture changes fundamentally when the experiments are performed at higher temperatures. At temperatures ≥ 50 °C, the biofilm and especially the EPS seems to dissolve partially if not completely resulting in large flocks of floating biofilm and very little still attached biofilm to the steel substrate. Consequently, the precipitation/scaling is different.

It seems that most of the scaling is stabilized in suspension and only a little is attached to the remaining biofilm/EPS or to the steel substrate. Turning back to the observations after the high temperature experiments, again and as already described above for the experiments performed at ambient temperature, an intense interaction between the (highly) branched networks of hyphae (filamentous structures) of *P. citrinum* can be observed (Figure 46).

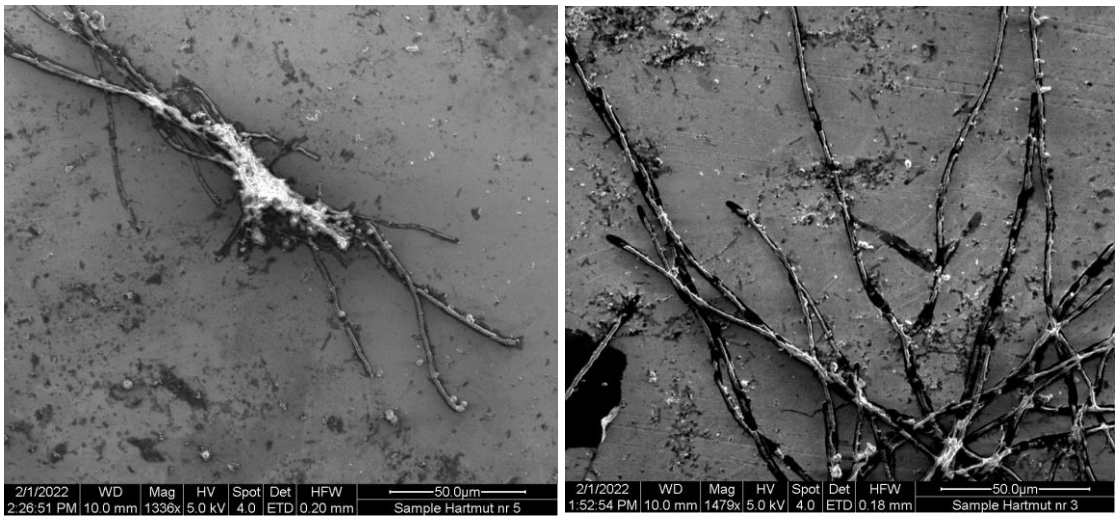

Figure 46: SEM pictures of the $CaCO_3$ precipitates/scaling formed at 50 °C after 1 hour reaction time on colonies of *Penicillium citrinum* covered areas of the biofilm on stainless steel substrates.

However, it appears that the coverage of the surface of the hyphae by $CaCO_3$ is somewhat less, the area in between is nearly free from scale. Looking to areas covered by biofilm of *Thermaerobacter sp.*, a similar picture occurs, nearly no $CaCO_3$ coverage of the plain bacteria (no EPS) can be observed. Only areas of colonies with remaining EPS show very small $CaCO_3$ scales with rather unspecific morphologies (Figure 47).

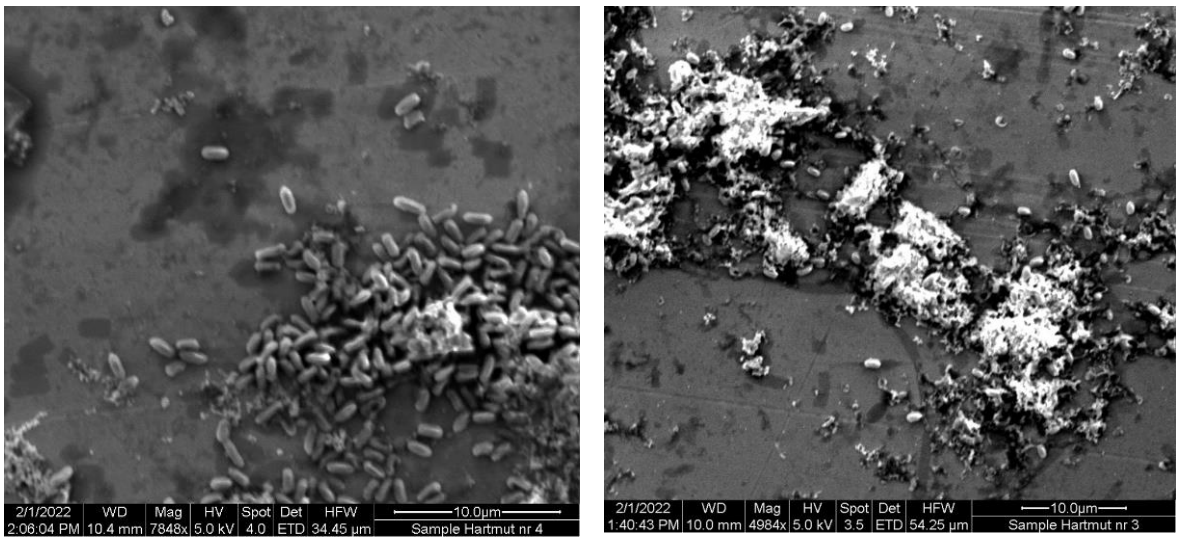

Figure 47: SEM pictures of the $CaCO_3$ precipitates/scaling formed at 50 °C after 1 hour reaction time on colonies of *Thermaerobacter sp*. covered areas of the biofilm on stainless steel substrates.

By inspection of a larger area of the substrate a mixture of morphologies can be seen, small $CaCO_3$ scales attached to the organic material and large crystals, possibly attached/precipitated from suspension and grown without interference of the biofilm (Figure 48).

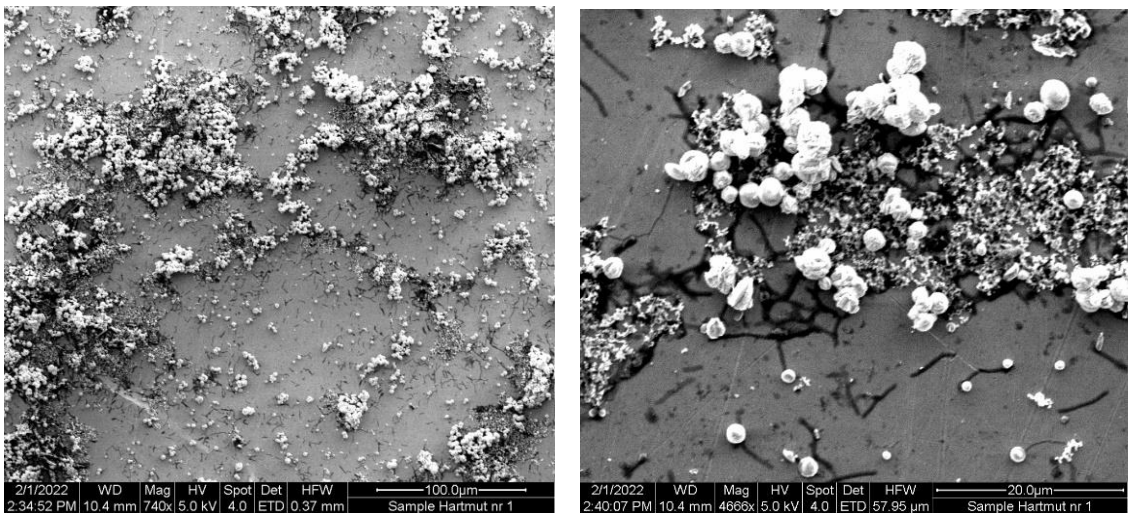

Figure 48: SEM pictures of the $CaCO_3$ precipitates/scaling formed at 50 °C after 1 hour reaction time on areas (partially) covered with the biofilm on stainless steel substrates.

Finally, areas with no biofilm (residues) only showed large $CaCO_3$ crystals of either calcite or vaterite morphologies most likely precipitated from suspension and/or grown directly on the steel substrate, just like shown in Figure 49.

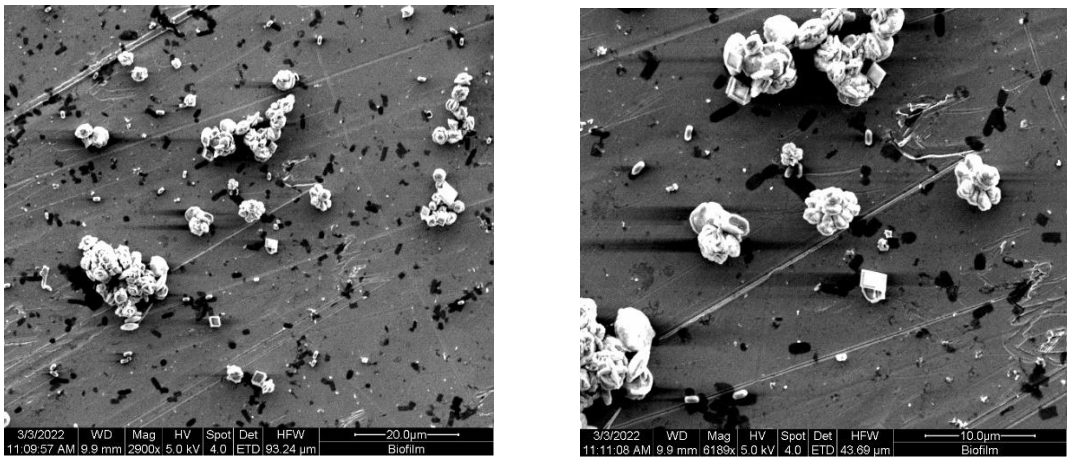

Figure 49: SEM pictures of the $CaCO_3$ precipitates/scaling formed at 50 °C after 1 hour reaction time on areas of the stainless-steel substrate with no biofilm (residues) coverage.

This experiment was also repeated/performed in the flow-loop set-up. Here the flow velocity was set to a minimal flow to avoid complete detachment of the biofilm due to the (partial) dissolution of the EPS at the elevated temperature (50 °C) and SR of 43 to get maximum production of nuclei to study the influence of the biofilm on nucleation and growth of $CaCO_3$ crystals.
Although the produced biofilms as depicted in Figure 28b are somewhat thick and hence an obstacle in the flow set-up, a complete detachment could be avoided during the experiment by choosing the minimal flow rate possible (30 ml/min).
After finishing the experiment and removal of the cover of the set-up containing the windows for inspection of the flow-loop when operated under pressure and elevated temperature, it became obvious, that extensive scale deposition occurred on areas with no biofilm attached and comparatively only limited deposition occurred on the biofilm covered areas (Figure 50).

Figure 50: Picture of the sample used in the flow-loop set-up after performing the experiment. Extensive scaling deposition (red encircled area) on blank steel areas are clearly present.

The goal of the experiment was a study of scale deposition on biofilm covered areas in time. However, due to the roughness of the sample, especially of the biofilm, a detailed kinetic assessment of the influence of the deposited biofilm on the formation of $CaCO_3$ scaling using the earlier successfully applied time resolved in-situ digital microscopy was not possible. A qualitative picture of the effect of the biofilm on the formation of $CaCO_3$ scaling can be drawn. The present biofilm, consisting possibly mostly of EPS and networks of hyphae (filamentous structures) of *P. citrinum* seems very dense and

covers (parts) of the steel substrate completely. These biofilm areas are covered almost completely with small, uniform sized $CaCO_3$ crystals after executing the experiment (Figure 51). Especially interesting is the intense interaction and the firm attachment of the $CaCO_3$ crystals onto the surface of the biofilm, the sample has been rinsed 5 times with de-ionised water before the SEM inspection was performed. However, the surface of the biofilm seems still to be completely covered with the $CaCO_3$ crystals.

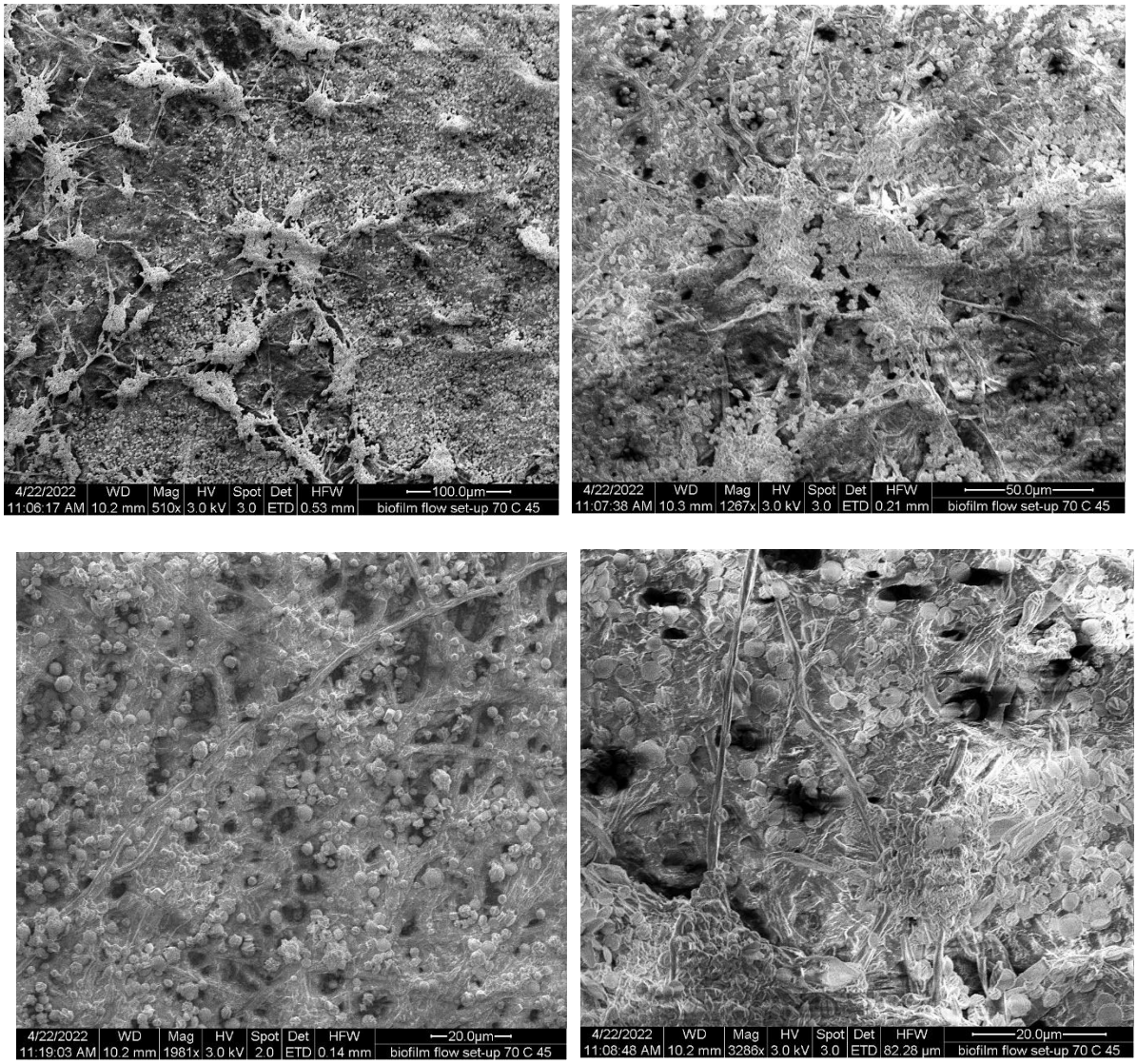

Figure 51: SEM pictures of the $CaCO_3$ precipitates/scaling formed at 50 °C after 1 hour reaction time in the flow-loop set-up on biofilm (EPS and networks of hyphae (filamentous structures) of *Penicillium citrinum*) covered areas of the stainless-steel substrate.

An inspection of biofilm free areas produced a similar and earlier described picture (Figure 52). A mixture of large calcite and vaterite crystals with rather 3-D morphology has been precipitated, clearly different from those attached to the biofilm covered areas.

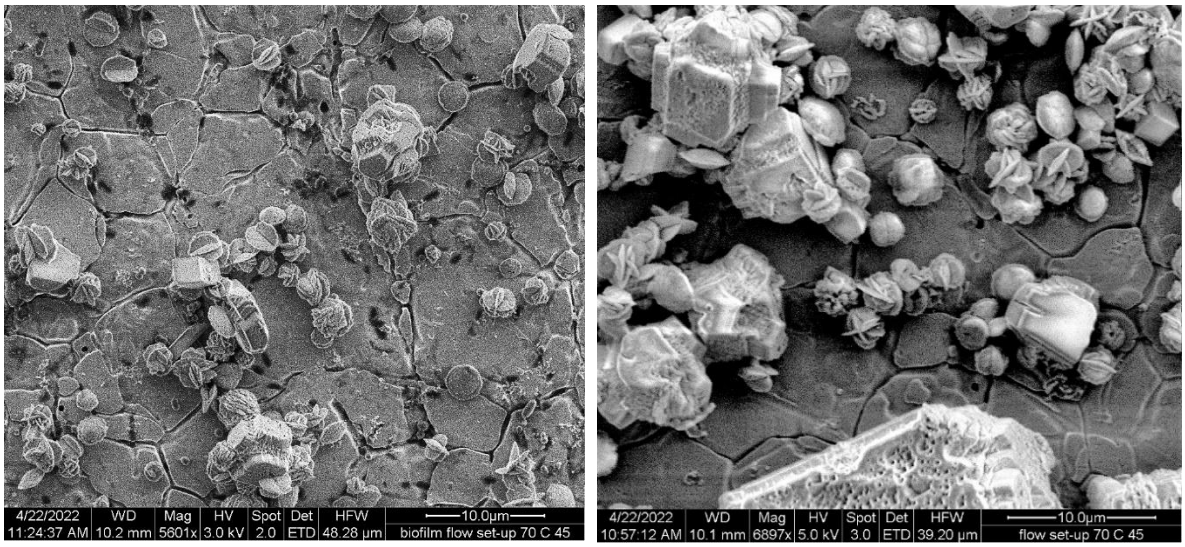

Figure 52: SEM pictures of the $CaCO_3$ precipitates/scaling formed at 50 °C after 1 hour reaction time in the flow-loop set-up on areas of the stainless-steel substrate with no biofilm (residues) coverage.

3.5 CONCLUSION PART II

The goal of this part of the project was to investigate the effect of a biofilm on the formation of calcium carbonate scale. From earlier studies it was known, that EPS can be involved in carbonate precipitation in different directions. Acidic polysaccharides may inhibit carbonate precipitation, on the other side EPS may transform upon decay into a highly organized template structure favoring calcium carbonate nucleation and as such enhancing precipitation of calcium carbonate where functional groups on EPS serve as initial nucleation sites.

The developed method using a small-scale dynamic set-up as well as a flow-loop set-up showed that partially the biofilm consisting of colonies of *Thermaerobacter* sp., *P. citrinum* and formed EPS dissolve in a flow configuration, especially at higher (≥ 50 °C) temperatures and therefore make detailed kinetic investigations impossible. Other microorganisms might be more suitable for flow through testing or a limitation of the grown biofilm thickness.

However, the biofilm components seem to develop intense interaction with the ions, nuclei and/or crystals formed during the executed experiments which could be shown by detailed microscopic studies. Also, it seems that the transformation of the intrinsically formed vaterite morphology to equilibrium calcite morphologies is delayed or hindered.

4 CONCLUSIONS

The aim of the WP 2.5.2 was the evaluation of the effect of organic compounds and microorganisms in formation and precipitation of colloids using artificial brines. UNINE provided the biological material (active and inactive bacteria/fungi) and a selection of organic compounds based on the analysis of the dissolved organic compounds from sampled fluids performed by GFZ was made. This was then used by TNO to perform experiments concerning scaling using dynamic light scattering (DSL). This method has proven to be a new approach to study important aspects of homogeneous nucleation like induction time and relative amounts of precipitate formed.

The first part concerned an investigation of the effect of several common carboxylic acids on the formation of homogeneous calcium carbonate scale. All carboxylic acids tested in this research had an inhibiting effect on the precipitation of calcium carbonate. Both the induction time and amount of precipitation was influenced by the carboxylic acids. An increase in concentration of acid groups resulted in an increase in induction time and a reduction in the total amount of scaling/precipitation. In most experiments conducted in this study no significant change in $CaCO_3$ crystal morphology was observed. Aragonite crystals was observed at several relatively highly acidic concentration experiments, normally only observed at high temperatures. DLS and SEM results showed that the presence of colloidal silica nanoparticles increased the formation of $CaCO_3$ precipitation and that many smaller crystals were formed around the silica nanoparticles.

The second part of the investigation was dedicated to evaluate the effect of a biofilm on the formation of calcium carbonate scales. From earlier studies it was known that EPS can be involved in carbonate precipitation. While acidic polysaccharides may inhibit carbonate precipitation, EPS may transform upon decay into a highly organized template structure favouring calcium carbonate nucleation, and as such, enhancing precipitation of calcium carbonate with functional groups on EPS serving as initial nucleation sites. The developed method using a small-scale dynamic set-up as well as a flow-loop set-up showed that partially the biofilm consisting of colonies of *Thermaerobacter* sp., *P. citrinum* and formed EPS dissolve in flow configuration, especially at higher (≥ 50 °C) temperatures and make detailed therefore kinetic investigations impossible.

However, the biofilm components seem to develop intense interaction with the ions, nuclei and/or crystals formed during the executed experiments, which could be shown by detailed microscopic studies. Also, it seems that the transformation of the intrinsically formed vaterite morphology to equilibrium calcite morphologies is delayed or hindered and extensive scaling is inhibited.

5 REFERENCES

1. Kieft, T.L., et al., *Dissolved organic matter compositions in 0.6–3.4 km deep fracture waters, Kaapvaal Craton, South Africa.* Organic Geochemistry, 2018. **118**: p. 116-131.
2. Sherwood Lollar, B., et al., *A window into the abiotic carbon cycle – Acetate and formate in fracture waters in 2.7 billion year-old host rocks of the Canadian Shield.* Geochimica et Cosmochimica Acta, 2021. **294**: p. 295-314.
3. Gioia, M.L.D., et al., *Occurrence of Organic Compounds in the Thermal Sulfurous Waters of Calabria, Italy.* Chromatographia, 2006. **63**(11): p. 585-590.
4. González-Barreiro, C., et al., *Occurrence of soluble organic compounds in thermal waters by ion trap mass detection.* Chemosphere, 2009. **75**(1): p. 34-47.
5. Butturini, A., et al., *Dissolved Organic Matter in Continental Hydro-Geothermal Systems: Insights from Two Hot Springs of the East African Rift Valley.* Water, 2020. **12**(12): p. 3512.
6. Lang, S.Q., et al., *Elevated concentrations of formate, acetate and dissolved organic carbon found at the Lost City hydrothermal field.* Geochimica et Cosmochimica Acta, 2010. **74**(3): p. 941-952.
7. Lang, S.Q., et al., *Deeply-sourced formate fuels sulfate reducers but not methanogens at Lost City hydrothermal field.* Scientific Reports, 2018. **8**(1): p. 755.
8. McDermott, J.M., et al., *Pathways for abiotic organic synthesis at submarine hydrothermal fields.* Proceedings of the National Academy of Sciences, 2015. **112**(25): p. 7668-7672.
9. Carothers, W.W. and Y.K. Kharaka, *Aliphatic acid anions in oil-field waters: implications for origin of natural gas.* Am. Assoc. Pet. Geol. Bull.; (United States), 1978. **62:12**: p. Medium: X; Size: Pages: 2441-2453 2009-12-16.
10. Kharaka, Y.K., et al., *Role of Organic Species Dissolved in Formation Waters from Sedimentary Basins in Mineral Diagenesis*, in *Roles of Organic Matter in Sediment Diagenesis*. 1985, SEPM Society for Sedimentary Geology. p. 0.
11. Hatton, R. and J. Hanor, *Dissolved volatile fatty acids in subsurface, hydropressure brines: a review of published literature on occurrence, genesis and thermodynamic properties. Technical Report for Geopressured-Geothermal Activities in Louisiana: Final Geological Report for the Period 1 November 1981 to 31 October 1982*. 1984, DOE
12. Kharaka, Y.K., T.H. Giordano, and P.D. Lundegard, *Distribution and Origin of Organic Ligands in Subsurface Waters from Sedimentary Basins*, in *Ore Genesis and Exploration: The Roles of Organic Matter*. 1997, Society of Economic Geologists. p. 0.
13. Sánchez-Avila, J.I., et al., *Distribution and origin of organic compounds in the condensates from a Mexican high-temperature geothermal field.* Geothermics, 2021. **89**: p. 101980.
14. Kompanichenko, V.N., V.A. Poturay, and G.A. Karpov, *Organic compounds in thermal water: The Mutnovskii area and the Uzon caldera.* Journal of Volcanology and Seismology, 2016. **10**(5): p. 305-319.
15. Poturay, V.A., *Organic matter in ground- and surface waters in the area of the Annenskii geothermal field, Russian Far East.* Geochemistry International, 2017. **55**(4): p. 393-400.
16. Vetter, A., *The influence of geothermal plants on the biogeochemistry of the microbial ecosystems in aquifers*, in *Technische Universität Berlin, Fakultät VI - Planen Bauen Umwelt*. 2012, Technische Universität Berlin: Berlin.
17. Westphal, A., et al., *Change in the microbial community of saline geothermal fluids amended with a scaling inhibitor: effects of heat extraction and nitrate dosage.* Extremophiles, 2019. **23**(3): p. 283-304.

18. Leins, A., et al., *Dissolved organic compounds in geothermal fluids used for energy production: a review.* Geothermal Energy, 2022. **10**(1): p. 9.
19. Glombitza, C., K. Mangelsdorf, and B. Horsfield, *A novel procedure to detect low molecular weight compounds released by alkaline ester cleavage from low maturity coals to assess its feedstock potential for deep microbial life.* Organic Geochemistry, 2009. **40**(2): p. 175-183.
20. Lovley, D.R. and F.H. Chapelle, *Deep subsurface microbial processes.* Reviews of Geophysics, 1995. **33**(3): p. 365-381.
21. Kharaka, Y.K. and J.S. Hanor, *Deep Fluids in the Continents: I. Sedimentary Basins.* Treatise on Geochemistry, 2003. **5**: p. 605.
22. Surdam, R., C. , et al., *Organic-Inorganic Interactions and Sandstone Diagenesis1.* AAPG Bulletin, 1989. **73**(1): p. 1-23.
23. Heperkan, D., et al., *Influence of temperature on citrinin accumulation by Penicillium citrinum and Peniccillium verrucosum in black table olives.* Toxin Reviews, 2009. **28**(2-3): p. 180-186.
24. Lebron, I. and D.L. Suarez, *Calcite nucleation and precipitation kinetics as affected by dissolved organic matter at 25°C and pH > 7.5.* Geochimica et Cosmochimica Acta, 1996. **60**(15): p. 2765-2776.
25. Lebrón, I. and D.L. Suárez, *Kinetics and Mechanisms of Precipitation of Calcite as Affected by PCO2 and Organic Ligands at 25°C.* Geochimica et Cosmochimica Acta, 1998. **62**(3): p. 405-416.
26. Kitano, Y. and D.W. Hood, *The influence of organic material on the polymorphic crystallization of calcium carbonate.* Geochimica et Cosmochimica Acta, 1965. **29**(1): p. 29-41.
27. Wada, N., K. Yamashita, and T. Umegaki, *Effects of Carboxylic Acids on Calcite Formation in the Presence of Mg2+ Ions.* J Colloid Interface Sci, 1999. **212**(2): p. 357-364.
28. Block, I.D. and F. Scheffold, *Modulated 3D cross-correlation light scattering: improving turbid sample characterization.* Rev Sci Instrum, 2010. **81**(12): p. 123107.
29. Meulendijks, N., et al., *Flow Cell Coupled Dynamic Light Scattering for Real-Time Monitoring of Nanoparticle Size during Liquid Phase Bottom-Up Synthesis.* Applied Sciences, 2018. **8**(1): p. 108.
30. Wray, J.L. and F. Daniels, *Precipitation of Calcite and Aragonite.* Journal of the American Chemical Society, 1957. **79**(9): p. 2031-2034.
31. Declet, A., E. Reyes, and O. Suárez, *Calcium carbonate precipitation: a review of the carbonate crystallization process and applications in bioinspired composites.* Reviews on Advanced Materials Science, 2016. **44**(1).
32. Sanni, O.S., *Calcium carbonate surface/bulk scaling mechanisms and kinetics in a once-through in-situ flow visualization rig*. 2016, University of Leeds.
33. Gargoum, L.A.M., *Calcium carbonate scale formation under multiphase turbulent conditions*. 2018, University of Leeds.
34. Eslinger, D.M. *Fighting Scale — Removal and Prevention*. 2000.
35. Rieger, J., et al., *Precursor structures in the crystallization/precipitation processes of CaCO3 and control of particle formation by polyelectrolytes.* Faraday Discussions, 2007. **136**(0): p. 265-277.
36. Goodwin, A.L., et al., *Nanoporous Structure and Medium-Range Order in Synthetic Amorphous Calcium Carbonate.* Chemistry of Materials, 2010. **22**(10): p. 3197-3205.
37. Görgen, S., et al., *The diversity of molecular mechanisms of carbonate biomineralization by bacteria.* Discover Materials, 2020. **1**(1): p. 2.
38. Lauchnor, E.G., et al., *Bacterially Induced Calcium Carbonate Precipitation and Strontium Coprecipitation in a Porous Media Flow System.* Environmental Science & Technology, 2013. **47**(3): p. 1557-1564.

39. Flemming, H.C. and J. Wingender, *The biofilm matrix.* Nat Rev Microbiol, 2010. **8**(9): p. 623-33.
40. Sheng, G.-P., H.-Q. Yu, and X.-Y. Li, *Extracellular polymeric substances (EPS) of microbial aggregates in biological wastewater treatment systems: A review.* Biotechnology Advances, 2010. **28**(6): p. 882-894.
41. Domozych, D., et al., *The extracellular polymeric substance of the green alga Penium margaritaceum and its role in biofilm formation.* Biofilms, 2005. **2**(2): p. 129-144.
42. Kawaguchi, T. and A.W. Decho, *A laboratory investigation of cyanobacterial extracellular polymeric secretions (EPS) in influencing CaCO3 polymorphism.* Journal of Crystal Growth, 2002. **240**(1): p. 230-235.
43. Arp, G., A. Reimer, and J. Reitner, *Calcification in cyanobacterial biofilms of alkaline salt lakes.* European Journal of Phycology, 1999. **34**(4): p. 393-403.
44. DeFarge, C., et al., *Texture of microbial sediments revealed by cryo-scanning electron microscopy.* Journal of Sedimentary Research, 1996. **66**(5): p. 935-947.
45. Giuffre, A.J., et al., *Polysaccharide chemistry regulates kinetics of calcite nucleation through competition of interfacial energies.* Proc Natl Acad Sci U S A, 2013. **110**(23): p. 9261-6.
46. Han, Z., et al., *Mechanism of Biomineralization Induced by Bacillus subtilis J2 and Characteristics of the Biominerals.* Minerals, 2019. **9**(4): p. 218.
47. Yee, N., et al., *The effect of cyanobacteria on silica precipitation at neutral pH: implications for bacterial silicification in geothermal hot springs.* Chemical Geology, 2003. **199**(1): p. 83-90.
48. Thompson, J.B. and F.G. Ferris, *Cyanobacterial precipitation of gypsum, calcite, and magnesite from natural alkaline lake water.* Geology, 1990. **18**(10): p. 995-998.
49. Douglas, S. and T.J. Beveridge, *Mineral formation by bacteria in natural microbial communities.* FEMS Microbiology Ecology, 1998. **26**(2): p. 79-88.
50. Ansari, A., et al., *Microbially-induced mineral scaling in desalination conditions: Mechanisms and effects of commercial antiscalants.* Water Research, 2020. **179**: p. 115863.
51. Perito, B., et al., *A Bacillus subtilis cell fraction (BCF) inducing calcium carbonate precipitation: Biotechnological perspectives for monumental stone reinforcement.* Journal of Cultural Heritage, 2014. **15**(4): p. 345-351.
52. Seifan, M. and A. Berenjian, *Microbially induced calcium carbonate precipitation: a widespread phenomenon in the biological world.* Applied Microbiology and Biotechnology, 2019. **103**(12): p. 4693-4708.
53. Braissant, O., et al., *Bacterially Induced Mineralization of Calcium Carbonate in Terrestrial Environments: The Role of Exopolysaccharides and Amino Acids.* Journal of Sedimentary Research, 2003. **73**(3): p. 485-490.
54. Maliszewska, I. and P. Mastalerz, *Production and some properties of lipase from Penicillium citrinum.* Enzyme and Microbial Technology, 1992. **14**(3): p. 190-193.
55. Ji, Y., et al., *Effect of water activity and temperature on growth of Penicillium citreoviride and Penicillium citrinum on MiGao (rice cake).* Can J Microbiol, 2007. **53**(2): p. 231-6.
56. Montani, M., et al., *Temperature influence on Penicillium citrinum thom growth and citrinin accumulation kinetics.* Int J Food Microbiol, 1988. **7**(2): p. 115-22.
57. Takai, K., A. Inoue, and K. Horikoshi, *Thermaerobacter marianensis gen. nov., sp. nov., an aerobic extremely thermophilic marine bacterium from the 11,000 m deep Mariana Trench.* Int J Syst Bacteriol, 1999. **49 Pt 2**: p. 619-28.
58. Spanevello, M.D., H. Yamamoto, and B.K.C. Patel, *Thermaerobacter subterraneus sp. nov., a novel aerobic bacterium from the Great Artesian Basin of Australia, and emendation of the genus Thermaerobacter.* Int J Syst Evol Microbiol, 2002. **52**(Pt 3): p. 795-800.